Available online at www.sciencedirect.com
ScienceDirect
Coordination Chemistry Reviews 250 (2006) 2308–2324
COORDINATION CHEMISTRY REVIEWS
www.elsevier.com/locate/ccr

Review

# Multi-frequency, high-field EPR as a powerful tool to accurately determine zero-field splitting in high-spin transition metal coordination complexes

J. Krzystek [a,*], Andrew Ozarowski [a], Joshua Telser [b]

[a] *National High Magnetic Field Laboratory, Florida State University, Tallahassee, FL 32310, USA*
[b] *Department of Biological, Chemical, and Physical Sciences, Roosevelt University, Chicago, IL 60605, USA*

Received 8 September 2005; accepted 6 March 2006
Available online 25 April 2006

## Contents



## Abstract

Electron paramagnetic resonance at multiple, high frequencies (95–700 GHz) and at correspondingly high magnetic fields (up to 25 T), known as HFEPR, is a relatively new technique. There have been an increasing number of applications of HFEPR, such as in organic radical chemistry and in materials science. The focus of this review, however, is on the application of HFEPR to transition metal coordination chemistry, in particular

*Abbreviations:* acac, anion of 2,4-pentanedione; bpea, *N*,*N*-bis(2-pyridylmethyl)-ethylamine; btz, 2,2′-bi-2-thiazoline; BWO, backward wave oscillator; cor, dianion of 8,12-diethyl-2,3,7,13,17,18-hexamethylcorrole; cyclam, 1,4,8,11-tetraazacyclotetradecane; dbm, dianion of 1,3-diphenyl-1,3-propanedione (dibenzoylmethane); dmb, 3,3-dimethyl-1-butanol; dmiz, 1,2-dimethylimidazole; DOTA, tetraazacyclododecanetetraacetic acid; DPDME, dianion of deuterioporphyrin IX dimethyl ester; DTPA, trianion of diethylenetriaminepentaacetic acid; EDTA, dianion of ethylenediaminetetraacetic acid; en, ethylenediamine; EPR, electron paramagnetic resonance; EtL, anion of 2-oxypropiophenone oxime; FDMRS, frequency-domain magnetic resonance spectroscopy; Gu, guanidinium; HFEPR, high-frequency and -field EPR; HIM2-py, 2-(2-pyridyl)-4,4,5,5-tetramethyl-4,5-dihydro-1*H*-imidazolyl-1-hydroxy; hmpH, 2-hydroxymethylpyridine; HS, high-spin; INS, inelastic neutron scattering; Im, imidazole; LS, low-spin; MCD, magnetic circular dichroism; NCTPP, trianion of 5,10,15,20-tetraphenyl-*N*-confused porphyrin; Pc, dianion of phthalocyanine; OEP, dianion of 2,3,7,8,12,13,17,18-octaethylporphyrin; Ph, phenyl; py, pyridine; taa, trianion of tris(1-(2-azolyl)-2-azabuten-4-yl(amine); $TBP_8Cz$, trianion of octa-*tert*-butylphenyl corrolazine; terpy, 2,2′:6′,2″-terpyridine; thf, tetrahydrofuran; SOC, spin–orbit coupling; SOD, superoxide dismutase; tpfc, trianion of 5,10,15-tris(pentafluorophenyl)corrole; TPP, dianion of 5,10,15,20-tetraphenylporphyrin; VTVH–MCD, variable temperature and field MCD; zf, zero-field; zfs, zf splitting

* Corresponding author. Tel.: +1 850 644 6077; fax: +1 850 644 1366.
*E-mail address:* krzystek@fsu.edu (J. Krzystek).


doi:10.1016/j.ccr.2006.03.016

to mononuclear complexes, as opposed to clusters that are relevant to single-molecule magnets. There are many complexes of paramagnetic transition metal ions for which conventional EPR (fields below 2 T, frequencies not exceeding 35 GHz) is less than ideal. Primarily, such systems are high-spin (i.e., $S > 1/2$), wherein the effects of zero-field splitting can make the complex either "EPR-silent" using conventional EPR, or make the EPR spectrum not particularly informative. Examples of the former are many integer-spin (non-Kramers) ions such as Mn(III) and Fe(II), while the latter case is exemplified by high-spin Fe(III). We will review here the use of HFEPR to study high-spin transition metal complexes, generally of the first row. For half-integer high-spin systems, we will review only those where the large magnitude of zero-field splitting necessitates the use of HFEPR. We will generally not discuss systems in which the zero-field splitting is in most cases very small and conventional EPR is extensively employed. The experimental and analytical methods for the accurate determination of zero-field splitting and other spin Hamiltonian parameters from HFEPR studies of these systems will be described. Comparison with other physical methods such as magnetometry, magnetic circular dichroism (MCD), and Mössbauer effect spectroscopy will also be made. We will further give selected examples how ligand-field theory can be used to provide information on chemical bonding and geometry, based on analysis of the spin Hamiltonian parameters well established by HFEPR.


*Keywords:* Coordination chemistry; Electron paramagnetic resonance; EPR; High-frequency and -field EPR; Magnetic resonance; Transition metal ions; Zero-field splitting

## 1. Introduction

It is well known that the electronic structure of metal complexes determines their magnetic properties. The reverse is also true to a certain extent—i.e., knowing the magnetic properties of a given complex may give us insight into its electronic structure, and sometimes its geometric structure as well. Knowledge of the magnetic properties of transition metal complexes is thus paramount in understanding various phenomena characteristic for them, such as catalytic activity. More recently, magnetism of such complexes have become of increased interest since it is relevant for the properties of "single-molecule magnets", which are polynuclear clusters assembled from mononuclear coordination complexes.

Transition ion complexes are often paramagnetic, since they have partly occupied d orbitals, and thus possess unpaired electron spins. The paramagnetism of such species makes them amenable to the electron paramagnetic resonance (EPR) experiment, which has been one of the most successful tools in investigating their magnetic properties [1]. From the point of view of coordination chemistry, octahedral $d^4$–$d^7$ transition metal complexes can be either low-spin (LS) or high-spin (HS). The former have the maximum number of paired electrons yielding spin ground states $S = 0$, 1/2, or 1 (respectively for $d^6$, $d^{5,7}$, $d^4$), and the latter have the maximum number of *un*paired electrons yielding $S = 3/2$, 2, or 5/2 (respectively for $d^7$, $d^{4,6}$, $d^5$) [2]. However, from the practical point of view of an EPR spectroscopist, *all* transition metal complexes can also be divided into two classes: low-spin (LS) and high-spin (HS), but in this context, LS means $S = 1/2$ (as $S = 0$ is diamagnetic and useless for EPR), while HS is any $S > 1/2$. HS complexes in turn can be segregated into half-integer spin numbers ($S = 3/2, 5/2$, etc.) and integer-spin numbers ($S = 1, 2$, etc.). As we will see below, the EPR properties of these three categories are distinctly different and each warrants a different experimental approach.

The main difference between the LS and HS complexes as defined for EPR lies in the phenomenon of zero-field splitting (zfs), which appears only for $S \geq 1$, i.e., in high-spin states. The admixture of excited electronic states to the ground state causes the different $M_S$ spin sublevels to split in the absence of a magnetic field in conditions of low symmetry. Zfs is mediated by spin–orbit coupling (SOC), and since the latter's magnitude varies strongly between different metal ions, and because of a variety of possible geometries, the zfs magnitudes vary accordingly, from very small values for highly symmetric complexes of Mn(II), where it is of the order of $10^{-2}$ cm$^{-1}$ to octahedral complexes of Co(II), where it is known to reach values of the order of $10^2$ cm$^{-1}$. While zfs of the magnitude lying at the lower end of the above range is usually easy to measure by conventional EPR, that approaching and exceeding the conventional EPR quantum energies ($\sim$0.3 cm$^{-1}$ for X-band and $\sim$1.2 cm$^{-1}$ for Q-band) is very difficult, and often impossible to determine using conventional methods, for reasons illustrated in Section 2.1. In view of this difficulty, most information on the magnetism of such problematic ions has been traditionally obtained from bulk magnetic susceptibility/magnetization measurements [1]. The accuracy of this bulk technique in determining spin Hamiltonian parameters in general, and zfs in particular, is, however, inferior to that of EPR, a resonance technique.

The recent decade has seen an impressive development in the extension of traditional EPR into high frequencies and fields (HFEPR) [3]. There are several excellent reviews of HFEPR in the literature; for the technical aspects we refer the reader to the review by Smith and Riedi [4]. For a review more relevant to the current topic, we refer to the paper of Hagen [5]. Compared to the latter, we will limit ourselves to HS transition ion complexes, although we will greatly expand the number of discussed systems due to the extensive progress in this technique since 1999. Of those, we will emphasize complexes where the large magnitude of zfs necessitates the use of HFEPR; non-Kramers (integer spin) species with very small zfs are left out, and so are those Kramers (half-integer spin) ions where the purpose of experiment has not been the measurement of zfs parameters. We note that zfs parameters can be determined by physical methods other than HFEPR. These range from well-known and widely applied magnetometric techniques, as mentioned above (e.g., variable temperature dc magnetic susceptibility) [6], to the very powerful, but less commonly used magneto-optic technique, magnetic circular dichroism (MCD) [7], to the rather exotic (for chemists) method, inelastic neutron scattering (INS) [8,9]. We also refer to the extensive review by Boča that lists zfs parameters for a wide range of transition metal

complexes, irrespective of the magnitude of zfs parameters or the experimental technique for their determination [10]. As discussed here and elsewhere [11], zfs parameters can be used to obtain valuable information on bonding in transition metal complexes through the use of ligand-field theory.

Lastly, we will not venture into the rapidly growing field of polynuclear ion clusters [12], which merit a separate review, but will restrict ourselves to mononuclear complexes. In the following section we will explain why HFEPR has been very successful in researching such complexes.

## 2. Methodology

### 2.1. Zero-field splitting of Kramers versus non-Kramers ions

The effect of zero-field splitting acting on the wavefunction representing the given high-spin state is usually treated using the spin Hamiltonian phenomenology. Such a spin Hamiltonian is represented in the following form:

$$H = \beta B\boldsymbol{g}S + B_2^0O_2^0 + B_2^2O_2^2 + B_4^0O_4^0 + B_4^2O_4^2 + B_4^4O_4^4 + \text{higher-rank terms} \quad (1a)$$

where $B_2^i$ ($i=0$, 2) are second-rank zfs terms, and $B_4^k$ ($k=0$, 2, 4 or $k=0$, 3 depending on symmetry) are fourth-rank zfs terms, $\beta$ is the Bohr magneton, $\boldsymbol{g}$ is the $g$-matrix. Other terms such as hyperfine coupling or nuclear quadruple interactions, or higher-rank Zeeman interactions, have been omitted.

Often, the same operator is written as follows:

$$H = \beta B\boldsymbol{g}S + D\left(S_z^2 - \frac{S(S+1)}{3}\right) + E(S_x^2 - S_y^2) + B_4^0O_4^0 + B_4^2O_4^2 + B_4^4O_4^4 \quad (1b)$$

where $D \equiv 3B_2^0$ and $E \equiv B_2^2$ are the more commonly used second-rank zfs parameters [13]. The fourth-rank zfs parameters come up only for $S \geq 3/2$, while sixth-rank parameters (omitted above) appear for $S \geq 3$. The operators $O_4^m$ as well as their matrix elements may be found in many texts including Abragam and Bleaney [1].

The effects of spin Hamiltonian defined in Eq. (1b) acting on the spin wavefunction vary depending on the spin number. Fig. 1 represents the spin sublevel energies calculated for the simplest HS Kramers ion, $S=3/2$, and the simplest HS non-Kramers ion, $S=1$. In both cases, the zfs tensor was assumed axial ($E=0$), and the parallel orientation of the zfs tensor relative to the Zeeman field was chosen. $D$ was set at 10 $cm^{-1}$, which is a typical value for HS transition ions, while arrows of two lengths represent quanta of EPR energy, shorter for Q-band (35 GHz, 1.2 $cm^{-1}$), and longer for W-band (95 GHz, 3.2 $cm^{-1}$). It follows from this figure that while – as a consequence of the Kramers theorem – for a half-integer spin species there appears within the $M_S=\pm1/2$ multiplet an allowed ($\Delta M_S=\pm1$) transition at any frequency, there is no such transition in an integer-spin system. To observe an allowed resonance in the latter case, an increase of operating frequency is necessary (from 35 to 95 GHz) assuming there is a limit on the magnetic field (in this case ~9 T, typical for superconducting magnets based on NbTi technology). Non-Kramers ions are thus often 'EPR-silent' at conventional conditions. It follows also from Fig. 1 that although a Kramers ion is, at least in principle, never 'EPR-silent', the intra-Kramers transitions within its $M_S=\pm1/2$, or other Kramers doublets are typically uninformative with regard to the zfs parameters, and it is much preferable to detect the inter-Kramers resonances. One such resonance appears near 9 T in this simulation, but is observable only at 95 GHz. Thus the common denominator for any attempt to determine the zfs of any HS transition ion, be it a Kramers, or non-Kramers species, characterized by large zfs parameters, is the application of HFEPR.

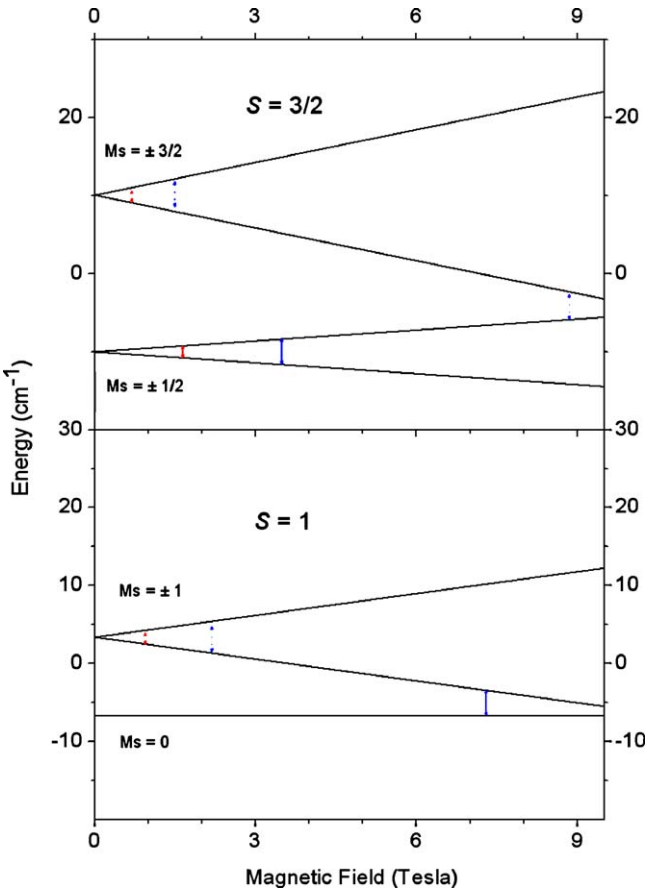


Fig. 1. Simulated spin sublevel energies as a function of magnetic field for the two simplest HS ions: $S=3/2$ (top, representing the Kramers class), and $S=1$ (bottom, representing the non-Kramers class). In both cases an axial zfs tensor was assumed, with $D=10\,cm^{-1}$, together with isotropic $g=2.00$. The shorter arrows represent the energy of a Q-band (35 GHz) microwave quantum while the longer arrows represent the energy of a W-band (95 GHz) quantum. Solid arrows indicate the formally magnetic-dipole allowed transitions, while dotted arrows represent the nominally forbidden resonances, which are often observed experimentally.

### 2.2. Extracting spin Hamiltonian parameters from HFEPR spectra

The methodology of extracting spin Hamiltonian parameters from HFEPR spectra has been initially the same as in conventional EPR: simulating the spectra using an initial set of spin

Hamiltonian parameters, comparing the simulations with experiment, and adjusting simulation parameters in an iterative process until a satisfactory agreement was found. If – as is often the case – the sample is polycrystalline or contained in a glass, the simulation process involves constructing a powder pattern, averaging over all spatial orientations of the single crystal with respect to the magnetic field [14].

The above described process is much more difficult for HS ions than for the LS species because of a more complex relationship between the resonance fields and the operating frequency in the former. Primarily for this reason, HFEPR experiments have, from early on, been performed at multiple frequencies, rather than at a single frequency [15]; another reason being that the commonly used and available sources (far-infrared lasers and Gunn oscillators) conveniently produced the required multiple frequencies. (Interestingly, the first example of a multi-frequency approach to HFEPR of HS transition ions dates back to the very early days of HFEPR in general [16]. Its discussion will be postponed until Section 3.7.) The agreement between simulation and experiment should be ideally the same at any frequency to verify the accuracy of the obtained parameters. However, this agreement was basically evaluated using human eye. In recent years, a more rationalized approach to extracting spin Hamiltonian parameters from multi-frequency data sets has been adopted [17,18]. Resonances detected at several frequencies are collected in a single two-dimensional (field versus frequency or energy) data set. This array is then simultaneously fitted to minimize the function:

$$\chi^2 = \sum_{i=1}^{N} (f_i^{(\mathrm{calc})} - f_i^{(\mathrm{exp})})^2 \tag{2}$$

where $f_i$ are the calculated and experimental resonance fields. This method assures that the parameters used in calculating the simulated resonances are truly optimized for any frequency, and allows the use of statistical methods to evaluate the experimental error $\sigma_i$, which is given by

$$\sigma_i = \sqrt{\frac{\chi^2}{N-P}(H^{-1})_{ii}} \tag{3}$$

where $N$ is the number of experimental resonances, and $P$ is the number of fitted parameters. $H$ is the Hessian matrix [19].

A yet more recent development has been reported by, among others, the authors of this review [20]. It depends on using quasi-continuously tunable frequency sources (BWOs), thus allowing one to record a given spectrum at any convenient frequency [21]. This methodology, being an extension of the multi-frequency approach, takes its advantage from the increased number of data points, which results in an increased accuracy of the derived spin Hamiltonian parameters according to Eq. (3). Equally important, it offers a possibility to tune in to true zf resonances, thus allowing one to quickly evaluate zfs parameters that serve as a starting point in the fitting procedures. Finally, the same methodology delivers not only the accurate zfs values, but also the **g**-matrix, which – as should be stressed – consists of intrinsic $g$-values, and not 'effective $g$'s' as has been customary until recently.

In the following section we will review the available literature on the principal subject of this paper. In doing so, we will categorize the discussed complexes in order of increasing d electronic configuration and location within the transition metal (d) block of the Periodic Table. Studies on selected f block ("rare earth") ions will also be mentioned.

## 3. Review of particular metal ions

### 3.1. V(III) ($d^2$, $S = 1$)

The ground-state electronic term for the free V(III) ion is $^3$F. An octahedral crystal/ligand field yields the ground orbital triplet $^3T_{1g}$, which is split by the additional trigonal ligand field into an orbital singlet $^3A_2$ and a doublet $^3$E. $^3A_2$ lies lower on the energy scale and becomes the ground electronic state. SOC gives rise to zfs of this spin-triplet state, which was early on evaluated as $8 \pm 1\,\mathrm{cm}^{-1}$ for $V^{3+}$ as a dopant in corundum through indirect methods [22]. These early years saw a rapid progression of sophisticated experiments on the same system. Thus, Foner and Low performed EPR at moderately high frequencies (36 and 71 GHz), but very high magnetic fields (up to 50 T), delivered by a pulsed magnet [23]. Under these conditions the detection of the allowed transitions within the triplet spin manifold was achieved, resulting in more accurate estimation of $D = 7.85\,\mathrm{cm}^{-1}$ and $g_{||} = 1.92$. Not long thereafter, Sauzade et al. delivered first true HFEPR spectra of $V^{3+}$ in corundum at 145 GHz [24]. Independently, Joyce and Richards [25] employed the FDMRS technique to further characterize the same system, obtaining $D = 8.25(2)\,\mathrm{cm}^{-1}$, $g_{||} = 1.92(3)$ and $g_\perp = 1.74(2)$.

The same octahedral $O_6$ donor set for V(III) was much more recently investigated in a series of very elegant studies by Tregenna-Piggott et al. on the hexaaqua ion $[V(H_2O)_6]^{3+}$ [17,26]. That ion was created by doping V(III) into the $CsGa(SO_4)_2{\cdot}12X_2O$ alum (X = H or D). This created a magnetically dilute system, in which the hyperfine structure of V(III) due to its nuclear spin $I = 7/2$ could be observed, and its constants determined [17]. The zfs tensor showed no indication of rhombicity, analogously to V(III) in corundum. Using multifrequency HFEPR, spin Hamiltonian parameters were determined with high accuracy, and found to be: $D = 4.7735(3)\,\mathrm{cm}^{-1}$, $E = 0$, $g_{||} = 1.9549(4)$, $g_\perp = 1.8690(5)$, $A_{||} = 0.0099(1)$ and $A_\perp = 0.0078(3)\,\mathrm{cm}^{-1}$ for the deuteriated alum, and $D = 4.8581(4)\,\mathrm{cm}^{-1}$, $E = 0$, $g_{||} = 1.9500(6)$, $g_\perp = 1.8656(4)$, $A_{||} = 0.0098(2)$ and $A_\perp = 0.0078(3)\,\mathrm{cm}^{-1}$ for the protonated species. In a following paper [27], a series of both neat, and doped alums were investigated. The neat (paramagnetic) complexes had the general formula: $M^I[Me^{III}(OX_2)_6](SO_4)_2$ where $M^I$ is one of the following ions: $[Cs(OX_2)_6]^+$, $[Rb(OX_2)_6]^+$, or $[C(NX_2)_3]^+$, X = H or D, and $Me^{III}$ = V(III). In doped (diamagnetic) complexes, $Me^{III}$ is a composite of V(III) and a diamagnetic (Group 13) tervalent ion: Al(III), Ga(III), or In(III). In all complexes, the zfs tensor remained axial. Small but significant variations of the axial zfs parameter $D$ were observed between various alums with the $M^I$ ion belonging to the Group 1, being in the 4.79–4.91 $\mathrm{cm}^{-1}$ range,

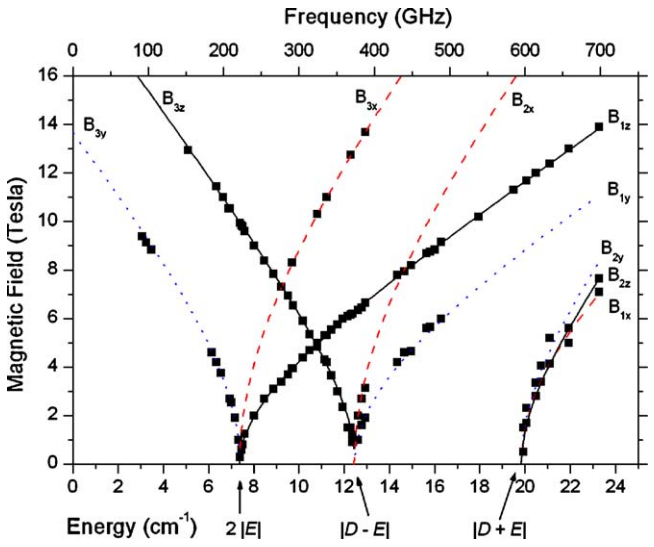


Fig. 2. Tunable-frequency EPR in an $S = 1$ system. Resonant field vs. quantum energy dependence for polycrystalline $VBr_3(thf)_3$ at 10 K. The squares are experimental HFEPR resonances while the curves were simulated using the best-fitted spin Hamiltonian parameters as in text, and in Table 1. Dashed lines represent $x$ turning points, dotted lines—$y$ turning points, and solid lines—$z$ turning points. The particular turning point branches are additionally identified using standard nomenclature for triplet states with rhombic symmetry. Three zf resonances are detected directly and marked with arrows.

with $g_{||} = 1.94(1)$ and $g_{\perp} = 1.87(1)$. A very different magnitude of the $D$ parameter was found in the complexes where the $M^I$ ion was the guanidinium ion, $D = 3.73\,cm^{-1}$, with $g_{||} = 1.94 \pm 0.01$ and $g_{\perp} = 1.90 \pm 0.02$. An exhaustive ligand-field analysis based on the AOM model was successfully used to bring into agreement the geometric, and electronic structures of the investigated complexes. In a following article [28], the dynamic Jahn-Teller effect was invoked to account for certain discrepancies that could not be explained previously. No HFEPR spectra could be obtained from the $[V(H_2O)_6]^{3+}$ cation in aqueous solution [29]. This observation has been confirmed by the authors of the current review. The reasons for the inability to observe HFEPR from frozen solution $[V(H_2O)_6]^{3+}$ have been carefully addressed by Dolder et al. [29]. They attribute this failure to strong $D$-strain leading to extensive inhomogeneous EPR linewidth broadening. This distribution in $D$ values results from distribution in the trigonal ligand field, which in turn results from only slight variation in the twist angle, $\varphi$, of the $H_2O$ ligands in hexaaqua complexes (see Fig. 2 in Dolder et al. [29]).

HFEPR observations of V(III) coordinated by a donor set other than $O_6$, and corresponding to true molecular coordination complexes are still very rare. The only work known to us so far is the paper of Krzystek et al. [30] on the series of three strongly distorted octahedral complexes: $V(acac)_3$, $VCl_3(thf)_3$ and $VBr_3(thf)_3$. The low symmetry of the complexes involved makes them completely 'EPR-silent' at conventional frequencies and fields, and necessitated the use of HFEPR. In the case of $V(acac)_3$, the donor set is still $O_6$, but the significant distortion results in a similar magnitude of $D$ as in the case of V(III) in corundum ($D = +7.470(1)\,cm^{-1}$) together with a strongly rhombic zfs tensor: $E = +1.916(1)\,cm^{-1}$, $E/D = 0.26$. The $g$-matrix was also determined: $g_x = 1.833(4)$, $g_y = 1.72(2)$, $g_z = 2.03(2)$. Of the two remaining complexes, representing the $X_3O_3$ (X = halide) donor set, $VBr_3(thf)_3$ resulted in highly accurate set of spin Hamiltonian parameters, obtained through the use of tunable-frequency EPR technique: $D = -16.162(6)\,cm^{-1}$, $E = -3.694(4)\,cm^{-1}$, $g_x = 1.86(1)$, $g_y = 1.90(1)$, $g_z = 1.710(4)$ (see Fig. 2). The magnitude of the zfs parameters is the highest ever measured by EPR for a triplet state, to the best of our knowledge, and represents the limits of the currently available instrumentation. The spin Hamiltonian parameters for the series of V(III) complexes were combined with a set obtained using the VTVH–MCD technique, and subsequently discussed in terms of the ligand-field theory, which correlated molecular structure with electronic structure.

### 3.2. V(II) ($d^3$, $S = 3/2$)

This relatively unstable oxidation state of vanadium is electronically similar to Cr(III) (see Section 3.3) and typically exhibits small zfs. For example, a V(II) site in corundum (formed by photoreduction of V(III) dopants via X-ray irradiation) gives $D = -0.160\,cm^{-1}$ [31]. As a result, X-band EPR can normally be used to determine zfs in V(II) complexes. An outstanding example is the work of Jacobsen et al. who studied complexes of general formula *trans*-$M(II)(py)_4X_2$, where M(II) = V(II) as a dopant and, e.g., Ru(II) as a host, and X = NCS, Cl, Br, I [32]. The zfs was nearly axial with $|D|$ in the range 0.19–0.37 $cm^{-1}$. We have recorded HFEPR spectra of frozen solution $[V(H_2O)_6]^{2+}$ at frequencies up to 330 GHz [33]. In this symmetrical complex, the zfs is small ($\sim$0.15 $cm^{-1}$) and the only effect of increasing frequency is a slight linewidth broadening due to $D$-(and/or $g$-)strain. No $^{51}V$ hyperfine splitting is resolved in HFEPR in this or in most other cases (for exceptions, see below).

### 3.3. Cr(III) ($d^3$, $S = 3/2$)

The ground-state electronic term for the free ion of this ubiquitous oxidation state of chromium is $^4F$. An octahedral crystal/ligand field yields the ground (orbital singlet) $^4A_{2g}$ state. SOC in conditions of low symmetry causes a splitting of this state into two Kramers doublets. The energy difference between them, i.e., the zfs is typically rather small, of the order of 0.38 $cm^{-1}$ in ruby [34], 0.191 in corundum [31], and 0.60 in $Cr(acac)_3$ [35], all with $O_6$ donor sets. Even in complexes of lower symmetry, such as the series *trans*-$[Cr(L)_4(X_2 \text{ or } XY)]^{n+}$, where L = $NH_3$, py; X, Y = F, Cl, Br, OH, $H_2O$; $1 \leq n \leq 3$, the $|D|$ values are generally $\sim$0.2 $cm^{-1}$ and only rarely exceed 0.4 $cm^{-1}$ [36]. Complexes of Cr(III) thus do not normally require HFEPR to determine their zfs parameters; the study by Pedersen and Toftlund employed both X- and Q-band frequencies [36]. A rare example of HFEPR on HS Cr(III) can be found in the paper of Shakurov and Tarasov [37], in which chromium was doped into single crystals of forsterite (a mineral of the formula $Mg_2SiO_4$). In these conditions Cr replaces Mg, creating several paramagnetic centers; one of them was attributed to HS Cr(III). The successful determination of zfs of Cr(III) in forsterite required the

use of moderately high EPR frequencies (65–85 GHz), but only conventional fields. The obtained spin Hamiltonian parameters are: $D = -0.978(17)\,cm^{-1}$, $E = -0.303(17)\,cm^{-1}$, $g_x = 1.95(2)$, $g_y = 2.06(2)$, $g_z = 1.82(2)$. It is noteworthy that the absolute sign of $D$ was determined to be negative, meaning that the $\pm 3/2$ Kramers doublet lies below the $\pm 1/2$ doublet in zero field, and that the zfs tensor is strongly rhombic ($E \sim 1/3\,D$).

### 3.4. Cr(II) ($d^4$, $S = 2$)

The ground-state electronic term for the free ion of this relatively rare oxidation state of chromium is $^5D$. An octahedral crystal/ligand field splits this term into a high-lying orbital triplet $^5T_{2g}$, and a low-lying orbital doublet $^5E_g$, which is Jahn-Teller-unstable, and undergoes splitting into the ground $^5B_{1g}$ and a higher-lying $^5A_{1g}$ state. The Jahn-Teller distortion in such a case corresponds to a tetragonal elongation. SOC in the conditions of low symmetry gives rise to zfs in the ground $^5B_{1g}$ state, splitting it into three (axial case) or five (rhombic case) spin sublevels.

The first measurement of zfs in Cr(II) was achieved remarkably early by Ono et al. on a single crystal of chromous sulfate pentahydrate ($CrSO_4{\cdot}5H_2O$; $O_6$ donor set), using several EPR frequencies up to 56 GHz [38,39]. The best fit between experiment and simulation was achieved for $D = 2.24\,cm^{-1}$, $E = 0.10\,cm^{-1}$, $g_\perp = 2.00$, $g_{||} = 1.96$. The small-magnitude rhombic component $E$ is noteworthy.

A much more extensive study was performed almost 50 years later by Tregenna-Piggott and coworkers on Tutton salts of the general formula $M^I[Cr^{II}(OX_2)_6](SO_4)_2$ where $M^I$ is one of the following ions: $NH_4^+$, $Rb^+$, or $Cs^+$, and X = H or D [9]. The species observed by HFEPR and related techniques, notably INS, was thus also Cr(II) with an $O_6$ donor set. The experiments were performed in an unusually broad temperature range (up to 250 K), and proved that the zfs is markedly temperature-dependent in these systems above 150 K. Thus, for the rubidium salt, $D = -2.411(1)\,cm^{-1}$, $E = -0.139(5)\,cm^{-1}$, $g_\perp = 1.995(5)$, $g_{||} = 1.96(2)$ at 10 K, and $D = -2.30(3)\,cm^{-1}$, $E = -0.185(5)\,cm^{-1}$, $g_\perp = 1.995(5)$, $g_{||} = 1.96(2)$ at 250 K. The decrease of $D$, and increase of $E$ with increasing temperature was similarly observed in all the systems studied, and explained by the dynamic Jahn-Teller effect. It is interesting to note that the zfs parameters obtained from HFEPR and INS differ in the high-temperature regime (above 150 K). This was explained by the motional averaging effects in EPR, and the different timescales of both experiments.

The hexaaqua Cr(II) complex was also an object of a HFEPR study by Telser et al. [40,41]. In contrast to the previously discussed experiments, this one was performed on the complex contained in aqueous low-temperature glass rather than on a single crystal. This brought as a result the following spin Hamiltonian parameters: $D = -2.20(5)\,cm^{-1}$, $E = 0.0(1)\,cm^{-1}$, $g_{iso} = 1.98(2)$ at 10 K. It is characteristic that the hexaaqua complex isolated in glass does not show the rhombic distortion appearing in the crystal. The subsequent ligand-field analysis underscored the role of low-lying excited triplet states in contributing to the zfs of the ground quintet.

Cr(II) coordinated to oxygen in octahedral environment was also studied as a dopant in the single crystal of forsterite by Tarasov et al. [42]. Two different sites were identified in the tunable-frequency (65–535 GHz) HFEPR spectra, and their zfs parameters were found to be: $D = -2.49\,cm^{-1}$, $E = 0.15\,cm^{-1}$ for the site termed 'M1', and $D = 2.23\,cm^{-1}$, $E = 0.4\,cm^{-1}$ for the site termed 'M2'. Similar studies, also employing tunable-frequency HFEPR, were performed on Cr(II) in a series of cubic fluoride crystals $Me^{II}F_2$, where $Me^{II}$ was Cd, Ca, Sr, and Ba [42,43]. A thorough data analysis allowed determining fourth-rank zfs parameters in addition to the usual second-rank terms. Thus, exemplary zfs parameters for the Cr(II) site in a $SrF_2$ single crystal are: $D = 2.790(3)\,cm^{-1}$, $E \approx 0.07\,cm^{-1}$, $B_4^0 = 4.0(6) \times 10^{-4}\,cm^{-1}$, $B_4^4 = 15.6(6) \times 10^{-4}\,cm^{-1}$ [44].

### 3.5. Mn(III) ($d^4$, $S = 2$)

The electronic structure of this ion is the same as that for Cr(II) (see above). There is a significant difference in terms of chemical stability as there is a large number of Mn(III) complexes and these are generally air-stable, while those of Cr(II) are very susceptible to air oxidation. Furthermore, an important subset of Mn(III) complexes comprises those with porphyrinic (tetrapyrrole) ligands, i.e., complexes of general formula Mn(P)X, where P is the dianionic porphyrin macrocycle and X is an axial, usually anionic ligand, such as Cl.

As a result, one of the first HFEPR studies of an integer-spin complex was of Mn(TPP)Cl, as well as other porphyrinic complexes (tetraazaporphyrins, known as porphyrazines) [45]. Mn(III) porphyrinic complexes appear to be particularly well suited towards investigation by HFEPR and a number of studies have been reported since then. These include not only true porphyrins [46–48], but also corrole complexes—a corrole being tetrapyrrole in which one of the four *meso* carbon atoms is missing [49,50]. More recently, HFEPR studies have been reported on a Mn(III) corrolazine complex (related to porphyrazine as corrole is related to porphyrin) [51], and on an "N-confused" (inverted) porphyrin (NCTPP; one with an $N_3C$ rather than $N_4$ donor set) [52].

The zfs parameters for Mn(III) in porphyrinic complex show relatively little variation, with the $-3 \le D \le -2\,cm^{-1}$ condition typically valid (see Table 1). True porphyrins are rigorously axial spin systems, and corroles and corrolazines show relatively little rhombic zfs, despite the lack of a $C_4$ rotation axis [49–51]. The primary outlier is $MnNCTPP(py)_2$, which has a relatively large magnitude, highly rhombic zfs: $D = -3.084$, $E = -0.608\,cm^{-1}$ [52]. In contrast to the other Mn(III) porphyrinic complexes, which are four- and five-coordinate, MnNCTPP is six-coordinate and it is possible that the zfs axis lies along the N–Mn–C direction, rather than normal to the porphyrin plane, as is the typically the case for Mn(P)X complexes.

Another important class of Mn(III) complexes are those with six-coordinate geometry derived from $[Mn(H_2O)_6]^{3+}$ and other complexes with oxygen donors, such as $Mn(acac)_3$ and related species. Indeed, a landmark study on EPR of Mn(III) was performed by Gerritsen and Sabisky on this ion as a dopant in rutile

Table 1
Summary of spin Hamiltonian parameters for high-spin transition metal ions obtained with HFEPR and related techniques

| Metal ion | Coord. sphere | Complex | $D$ (cm$^{-1}$) | $E$ (cm$^{-1}$) | $g_x$ | $g_y$ | $g_z$ | Reference |
|---|---|---|---|---|---|---|---|---|
| V(III), d$^2$, $S=1$ | $O_6$ | V(III) doped into $Al_2O_3$ | +7.85 | 0 | | | 1.92 | [23] |
| | $O_6$ | V(III) doped into $Al_2O_3$ | 8.29(2) | 0 | | | | [24] |
| | $O_6$ | V(III) doped into $Al_2O_3$ | 8.25(2) | 0 | 1.74(2) | 1.74(2) | 1.92(3) | [25] |
| | $O_6$ | $V(H_2O)_6^{3+}$ in $RbGa(SO_4)_2\cdot 12H_2O$[a] | 4.906(4) | 0 | 1.863(2) | 1.863(2) | 1.944(1) | [26] |
| | $O_6$ | $V(D_2O)_6^{3+}$ in $CsGa(SO_4)_2\cdot 12D_2O$[b] | 4.7735(2) | 0 | 1.8690(2) | 1.8690(2) | 1.9549(1) | [27] |
| | | $V(H_2O)_6^{3+}$ in $CsGa(SO_4)_2\cdot 12H_2O$[c] | 4.8581(4) | 0 | 1.8656(2) | 1.8656(2) | 1.9500(5) | [17] |
| | | $V(H_2O)_6^{3+}$ in $GuGa(SO_4)_2\cdot 12H_2O$[d] | 3.393(3) | 0 | 1.895(1) | 1.895(1) | 1.960(1) | [27] |
| | $O_6$ | $V(acac)_3$ | +7.470(1) | +1.916(1) | 1.833(4) | 1.72(2) | 2.03(2) | [30] |
| | $O_3Br_3$ | $VBr_3(thf)_3$ | −16.162(6) | −3.694(4) | 1.86(1) | 1.90(1) | 1.710(4) | [30] |
| Cr(III), d$^3$, $S=3/2$ | $O_6$ | Cr doped into $Mg_2SiO_4$ | −0.98(2) | −0.30(2) | 1.95(2) | 2.05(2) | 1.82(2) | [37] |
| Cr(II), d$^4$, $S=2$ | $O_6$ | $Cr(H_2O)_6^{2+}$ in $CrSO_4\cdot 5H_2O$ | 2.24 | 0.1 | 2.00 | 2.00 | 1.96 | [38,39] |
| | $O_6$ | $Cr(H_2O)_6^{2+}$ in solution | −2.20(5) | 0.0(1) | 1.98(2) | 1.98(2) | 1.98(2) | [40,41] |
| | $O_6$ | Cr doped into $Mg_2SiO_4$ | | | | | | [42] |
| | | Site M1 | −2.49 | 0.15 | | | | |
| | | Site M2 | 2.23 | 0.4 | | | | |
| | $O_6$ | $Rb_2[Cr(D_2O)_6](SO_4)_2$[e] | | | | | | [9] |
| | | $T=10$ K | −2.411(1) | 0.139(1) | 1.995(5) | 1.995(5) | 1.96(2) | |
| | | $T=250$ K | −2.30(3) | 0.185(5) | 1.995(5) | 1.995(5) | 1.96(2) | |
| | $F_8$ | Cr doped into $SrF_2$[f] | 2.790(3) | ∼0.07 | 1.96(1) | 1.98(1) | 1.94(1) | [44] |
| Mn(III), d$^4$, $S=2$ | $O_6$ | $Mn^{3+}$ doped in $TiO_2$ | −3.4(1) | 0.116(1) | 2.00(2) | 2.00(2) | 1.99(1) | [53] |
| | $O_6$ | $Mn(dbm)_3$ | −4.35 | 0.26 | 1.99 | 1.99 | 1.97 | [54] |
| | $O_6$ | $Mn(acac)_3$ | −4.52(2) | 0.25(2) | 1.99(1) | 1.99(1) | 1.99(1) | [55] |
| | $O_6$ | $CsMn(SO_4)_2\cdot 12D_2O$[g] | −4.524(1) | 0.276(1) | | | | [118] |
| | $O_6$ | $CsMn(SO_4)_2\cdot 12D_2O$ | −4.491(7) | 0.248(5) | 1.981(5) | 1.993(5) | 1.988(5) | [18] |
| | $O_6$ | $CsMn(SO_4)_2\cdot 12H_2O$ | −4.431(9) | 0.258(8) | 2.001(5) | 1.997(7) | 1.966(12) | [18] |
| | $O_6$ | $Mn(H_2O)_6^{3+}$ in $CsGa(SO_4)_2\cdot 12H_2O$[h] | −4.514(1) | −0.161(5) | 2.000(1) | 2.000(1) | 1.9844(6) | [58] |
| | $O_6$ | $[Mn(dbm)_2(CH_3OH)_2]Br$ | −3.46 | 0.13 | 1.99 | 1.99 | 1.99 | [11] |
| | $O_4Cl$ | $Mn(Me_2dbm)Cl$ | −2.45(3) | 0.00(1) | 2.03(2) | 2.03(2) | 2.02(2) | [59] |
| | $O_4Br$ | $Mn(Me_2dbm)Br$ | −1.40(2) | 0.00(1) | 1.98(2) | 1.98(2) | 1.98(2) | [59] |
| | $N_2O_4$ | $[Mn(dbm)_2(py)_2](ClO)_4$ | −4.504(2) | −0.425(1) | 1.993(1) | 1.994(1) | 1.983(1) | [56] |
| | $N_2O_2Cl$ | Mn(salen) | −2.47(2) | 0.17(1) | 2.00(2) | 2.00(2) | 2.00(2) | [48] |
| | $N_3F_3$ | $Mn(terpy)F_3$ | −3.82(2) | 0.75(2) | 1.97(2) | 2.04(1) | 1.96(1) | [62] |
| | $N_3F_3$ | $Mn(bpea)F_3$ | −3.67(2) | 0.70(2) | 1.96(1) | 1.98(1) | 1.98(1) | [62] |
| | $N_4$ | Mn(cor) | −2.64(1) | 0.015(5) | 2.02(1) | 2.02(1) | 2.00(1) | [50] |
| | $N_4O$ | $(TBP_8Cz)Mn\cdot CH_3OH$ | −2.60(2) | 0.015(5) | 2.00(1) | 2.00(1) | 2.00(1) | [51] |
| | $N_4O$ | $Mn(tpfc)(OPPh_3)$ | −2.69(2) | 0.030(3) | 1.994(4) | 1.994(4) | 1.980(4) | [49] |
| | $N_4Cl$ | Mn(TPP)Cl[j] | −2.290(5) | 0.00(1) | 2.005(5) | 2.005(5) | 1.98(2) | [46] |
| | $N_4Cl$ | Mn(Pc)Cl | −2.31(1) | 0.00(1) | 2.005(5) | 2.005(5) | 2.00(2) | [46] |
| | $N_4Cl$ | Mn(TSP)Cl | −3.12(2) | 0.00(1) | 2.00(2) | 2.00(2) | 2.00(2) | [48] |
| | $N_4Cl$ | Mn(DPDME)Cl[i] | −2.53(2) | <0.013 | | | | [86] |
| | $N_4Cl$ | Mn(OEP)Cl | −2.40(1) | ≤0.02(1) | 2.00(1) | 2.00(1) | 2.00(1) | [59] |
| | $N_4Br$ | Mn(DPDME)Br[i] | −1.1(1) | ∼0 | | | | [86] |
| | $N_4Br$ | Mn(OEP)Br | −1.07(1) | 0.00(1) | 2.01(1) | 2.01(1) | 1.98(1) | [59] |
| | $N_4Br_2$ | [Mn(cyclam)Br$_2$]Br[k] | −1.1677(7) | −0.0135(6) | 2.005(4) | 2.036(2) | 2.015(2) | [64] |
| | $N_4I_2$ | $Mn(cyclam)I_2$ | +0.604 | 0.034 | 2.00 | 2.00 | 1.99 | [63] |
| | $N_5$ | Mn(cor)(py) | −2.78(1) | 0.030(5) | 2.02(1) | 2.02(1) | 2.00(1) | [50] |
| | $N_5$ | $Mn(DPDME)N_3$[i] | −3.1(1) | <0.12 | | | | [86] |
| | $N_5C$ | $Mn(NCTPP)(py)_2$ | −3.08 | −0.61 | 2 | 2 | 2 | [52] |
| | $N_6$ | $Mn(terpy)(N_3)_3$ | −3.29(1) | 0.51(1) | 2.000(5) | 1.980(5) | 2.010(5) | [61] |
| | $N_6$ | $Mn(bpea)(N_3)_3$ | +3.50(1) | 0.82(1) | 2.02(1) | 1.98(1) | 1.95(1) | [62] |
| | $N_6$ | Mn(taa) | −5.90 | 0.50 | 2.0 | 2.0 | 2.0 | [60] |
| Mn(II), d$^5$, $S=5/2$ | $N_4$ | Mn protoporphyrin IX | 0.775 | 0.037 | 2.001 | 2.001 | 2.001 | [67] |
| | $N_4X_2$ | $Mn(o\text{-phen})_2X_2$[l] | | | | | | [67] |
| | | X = Cl | 0.124 | 0.005 | 2.000 | 2.000 | 2.000 | |
| | | X = Br | 0.359 | 0.074 | 2.002 | 2.002 | 2.002 | |
| | | X = I | 0.590 | 0.145 | 2.008 | 2.008 | 2.008 | |
| | $P_2X_2$ | dichlorobis(triphenylphosphine oxide)Mn(II) | 0.165(1) | 0.045(1) | 2.0000(6) | 2.0000(6) | 2.0000(6) | [68] |
| | | dibromobis(triphenylphosphine oxide)Mn(II) | 0.507(1) | 0.134(1) | 1.9985(3) | 1.9985(3) | 1.9985(3) | |
| | | diiodobis(triphenylphosphine oxide)Mn(II) | 0.906(1) | 0.223(1) | 0.223(1) | 2.0039(3) | 2.0039(3) | |

Table 1 (*Continued*)

| Metal ion | Coord. sphere | Complex | $D$ ($cm^{-1}$) | $E$ ($cm^{-1}$) | $g_x$ | $g_y$ | $g_z$ | Reference |
|---|---|---|---|---|---|---|---|---|
| | $N_3X_2$ | $Mn(terpy)X_2$ | | | | | | [73] |
| | | X = I | +1.000(5) | 0.19(1) | 1.98(2) | 1.99(2) | 1.97(2) | |
| | | X = Br | +0.605(5) | 0.159(1) | 1.985(10) | 1.975(10) | 1.965(10) | |
| | | X = Cl | −0.26(2) | 0.075(5) | 1.994(5) | 2.010(7) | 2.025(5) | |
| | | X = SCN | −0.30(1) | 0.050(5) | 1.99(2) | 1.97(2) | 1.97(1) | |
| | $N_3O_2$ | MnSOD[m] | 0.3588 | 0.0146 | 2.00092 | 2.00092 | 2.00092 | [76] |
| Fe(III), $d^5$, $S = 5/2$ | $O_6$ | Fe in $PbTiO_3$ | 1.176 | 0 | 2.002 | 2.002 | 2.002 | [89] |
| | $O_6$ | Fe doped in $Al_2O_3$ | 0.1683 | 0 | 2.003 | 2.003 | 2.003 | [92] |
| | $O_6$ | Fe in $Al_2O_3$-hercynite pigment | 0.1850 | 0.00159 | 2.002 | 2.002 | 2.002 | [90] |
| | $N_2O_4$ | Fe(III)-EDTA | 0.8 | 0.27 | | | | [81] |
| | $N_4X$ | Deutero porphyrin IX dimethyl ester X (X = axial ligand)[i] | | | | | | [86] |
| | | X = F | 5.5(1) | | | | | |
| | | X = Cl | 8.95(18) | ∼0 | | | | |
| | | X = Br | 11.8(2) | ∼0 | | | | |
| | | X = I | 16.4(2) | ∼0 | | | | |
| | $N_4F$ | Myoglobin-fluoride complex | ∼5.0 | 0 | | | | [81] |
| | $N_4O$ | Met-hemoglobin | 10.7(2) | | 1.95(1) | 1.95(1) | | [16] |
| | $N_4O$ | Met-myoglobin | 9–9.5 | 0 | 1.98 | 1.98 | | [80] |
| | $S_6$ | Tris(pyrrolidyl dithiocarbamato)Fe(III)[i] | −2.14(5) | 0.21(1) | | | | [86] |
| Fe(II), $d^6$, $S = 2$ | $O_6$ | $Fe(H_2O)_6^{2+}$ in $FeSiF_6 \cdot 6H_2O$[i] | 11.78 | 0.67 | | | | [95] |
| | $O_6$ | $[Fe(H_2O)_6](ClO_4)_2$ | +11.34(4) | +0.69(1) | 2.18(1) | 2.18 | 2.023(6) | [93] |
| | $O_6$ | $(NH_4)_2[Fe(H_2O)_6](SO_4)_2$ | +14.94(2) | +3.778(2) | 2.226(6) | 2.31(1) | 1.93(3) | [93] |
| | $O_6$ | $[Fe(H_2O)_6]SO_4 \cdot H_2O$ | +10.32(1) | +2.23(1) | 2.10(1) | 2.04(1) | 2.11(1) | [93] |
| | $N_6$ | $Fe(bithiazoline)_2(SCN)_2$ | +12.427(12) | +0.243(3) | 2.147(3) | 2.166(3) | 2.01(1) | [94] |
| | $S_4$ | $[PPh_4]_2[Fe(SPh)_4]$[i] | 5.98 | 1.42 | | | | [95] |
| | $S_4$ | $[PPh_4]_2[Fe(SPh)_4]$ | +5.84 | 1.42 | 2.08 | 2.08 | 2.00 | [96] |
| Co(II), $d^7$, $S = 3/2$ | $X_4$ | $Cs_3CoX5$ | | | | | | [101] |
| | | X = Cl | −4.30(4) | 0 | 2.30(2) | 2.30(2) | 2.40(2) | |
| | | X = Br | −5.3(1) | 0 | 2.32 | 2.32 | 2.42 | |
| | $P_2Cl_2$ | $Co(PPh_3)_2Cl_2$ | −14.76(2) | 1.141(8) | 2.166(4) | 2.170(4) | 2.240(5) | [102] |
| Ni(II), $d^8$, $S = 1$ | $O_6$ | $Ni(H_2O)_6^{2+}$ in $NiSO_4 \cdot 7H_2O$ | −3.5 | −1.5 | 2.2 | 2.2 | 2.2 | [106] |
| | $O_4N_2$ | [Ni(oxalate)-(dmiz)$_2$] | 1.875(4) | 0.38(4) | 2.222(1) | 2.216(1) | | [110] |
| | $O_4NCl$ | $Ni(hmp)_4(dmb)_4Cl_4$ | −5.30(5) | 1.20(2) | 2.20(5) | 2.20(5) | 2.30(5) | [111] |
| | $N_4O_2$ | $[Ni(EtL)_2(Me_5dien)]$ | 2.98 | 0.69 | 2.165 | 2.175 | 2.150 | [107] |
| | $N_4O_2$ | $[Ni\text{-}(HIM2\text{-}py)_2NO_3]NO_3$ | −10.1 | 0.02(1) | 2.17 | 2.17 | 2.17 | [114] |
| | $N_6$ | $Ni^{2+}$ in $Zn(en)_3(NO_3)_2$ | 0.832 | 0 | 2.156 | 2.156 | 2.181 | [108] |
| | $N_6$ | $[Ni(5\text{-methylpyrazole})_6](ClO_4)_2$ | | | | | | [107] |
| | | $T = 295$ K | 0.41 | 0 | 2.178 | 2.178 | 2.178 | |
| | | $T = 100$ K | 0.72 | 0 | 2.178 | 2.178 | 2.178 | |
| | $N_6$ | $[Ni(5\text{-methylpyrazole})_6](BF_4)_2$ | | | | | | |
| | | $T = 295$ K | 0.48 | 0 | 2.178 | 2.178 | 2.178 | [107] |
| | | $T = 100$ K | 0.54 | 0 | 2.178 | 2.178 | 2.178 | |
| | $N_6$ | $[Ni(sarcophagine)](ClO_4)_2$ | +1.400 | 0 | 2.143(1) | 2.143(1) | 2.125(1) | [109] |
| | $P_2Cl_2$ | $Ni(PPh_3)_2Cl_2$ | +13.196(2) | +1.848(6) | 2.200(5) | 2.177(1) | 2.15(1) | [20] |
| Gd(III), $f^7$, $S = 7/2$ | $O_6$ | Gd doped in $Al_2O_3$ | 0.1033 | 0 | 2.003 | 2.003 | 2.003 | [92] |

[a] Isotropic hyperfine coupling constant for $^{51}V$ was also found to be 111(2) G.

[b] Anisotropic hyperfine coupling constants for $^{51}V$ were also found to be: $A_{||} = 99 \times 10^{-4}\ cm^{-1}$, $A_{\perp} = 78 \times 10^{-4}\ cm^{-1}$.

[c] V(III) was also doped in a large variety of different alums; parameters, including anisotropic hyperfine coupling constants, are reported in original work.

[d] Another site of different symmetry yielded slightly varying spin Hamiltonian parameters.

[e] A series of Tutton's salts of the general formula: $M^I[Cr^{II}(OX_2)_6](SO_4)_2$, where $M^I = NH_4^+$, $Rb^+$, or $Cs^+$, and X = H or D, was studied.

[f] Fourth-rank zfs parameters were also obtained. Cr(II) doped in other cubic $MeF_2$ (Me = Ca, Cd, Ba) crystals was also investigated by Tarasov and coworkers [43,119].

[g] A zf INS experiment.

[h] Fourth-rank zfs parameters, and anisotropic hyperfine coupling constants for $^{55}Mn$ were reported: $A_{xx} = A_{yy} = -0.0087(2)\ cm^{-1}$, $A_{zz} = -0.00531(5)\ cm^{-1}$.

[i] A zf FDMRS experiment.

[j] A series of related porphyrazinato Mn(III) complexes was also studied in the earlier study [45].

[k] Fourth-rank zfs parameters were also determined in this single-crystal study.

[l] An analogous series of complexes: $[MnL_4X_2$ or $Mn(L\text{–}L)_2X_2]$, where L = γ-picoline, L–L = *o*-phenanthroline; X = Cl, Br, I, was also studied and the same trend of increasing $D$ observed.

[m] A large variety of MnSOD enzymes originating from different sources was investigated in the quoted paper, and also in [75,77].

($TiO_2$; $O_6$ donor set) [53]. One of the first HFEPR studies of a transition metal complex was by Barra et al. on $Mn(dbm)_3$ [54]. In this type of complex, the magnitude of zfs is larger ($-4.5\,cm^{-1}$ versus $-2\,cm^{-1}$) and the tensor more rhombic than in porphyrin complexes (see Table 1). Since then, other complexes of this general type have been studied by HFEPR, such as $Mn(acac)_3$ itself [55] and other complexes partly with diketonate coordination [11,56]. The study on $Mn(acac)_3$ presents an interesting example of the utility of HFEPR for providing structural information. As mentioned above for Cr(II), crystal-field theory gives the result that for tetragonally elongated octahedral $d^4$, the ground state is $^5B_{1g}$, while for tetragonal compression, the ground state is $^5A_{1g}$. In the former case, the sign of $D$ is negative, while for the latter $D$ is positive. Two crystal structures for $Mn(acac)_3$ had been reported and in one case there was tetragonal elongation, and in the other compression. A magnetic susceptibility study of $Mn(acac)_3$ reported a positive value for $D$ [57]. A HFEPR study of $Mn(acac)_3$ in the solid state clearly demonstrated that $D$ was negative, and more importantly, that in frozen solution $D$ was negative as well, based on simulations of variable temperature spectra [55]. Thus, HFEPR proved that in frozen solution, free of crystal packing effects, the "natural" Jahn-Teller effect on $Mn(acac)_3$ is tetragonal elongation. Another Mn(III) complex with an $O_6$ donor set has been studied by HFEPR: the hexaaqua ion in alums [18,58], which gave zfs parameters very close to those for $Mn(acac)_3$ and related complexes. The very recent study by Krivokapič et al. was on single crystals (as well as powders) of Mn(III) doped into a CsGa alum. Hyperfine splitting from $^{55}Mn$ was nicely resolved, which gave both $A_\perp$ and $A_{||}$ values, along with zfs terms through fourth-rank [58]. Thus far, the only cases in which hyperfine splitting from suitable nuclei (i.e., 100% abundance of a magnetically active nucleus, e.g., $^{51}V$, $^{55}Mn$, $^{59}Co$) has been observed in non-Kramers systems by HFEPR is in doped single crystals [26,58], or a doped powder [58], but never in frozen solution, in contrast to conventional EPR, where hyperfine splitting is routinely resolved in frozen solution, as well as in doped powders. Presumably, $D$-strain (and even $A$-strain) from conformational distribution leads to insurmountable line broadening, obscuring hyperfine splitting.

A variety of other complexes of Mn(III) have been studied by HFEPR, including those with chelating O,N-donor (salen type) [48,59] and other N-donor ligands [60–62]. Among the latter are complexes of general formula $[Mn(L–L–L)X_3]$, where L–L–L = bpea, terpy; X = $N_3$, F. These studies also present a nice example of structural correlations from zfs parameters determined by HFEPR. Crystal structures of the Mn(III) complexes of bpea and terpy with X = F both show tetragonal elongation and negative values for $D$, while the complex with bpea and X = $N_3$ shows a structural compression and a positive value for $D$.

However, as shown by Mossin et al. [63], the above structural correlation is not foolproof. For the complex $[Mn(cyclam)I_2]I$, the value for $D$ is positive, $+0.604\,cm^{-1}$ (with $|E| = 0.034\,cm^{-1}$), far out of range from other six-coordinate Mn(III) complexes with tetragonal elongation (or from five-coordinate complexes, which can be considered as an extreme case of this type). This was described as resulting from a substantial contribution of a ligand-to-metal charge transfer (LMCT) excited state that can be represented in simplified fashion as $[Mn(II)I^\bullet]^{2+}$ ($d^1_{xy}d^1_{yz}d^1_{xz}d^2_{z^2}5p^5$), corresponding to $^4B_1 \otimes {}^2P$ (in $C_{4v}$ symmetry), as opposed to the "pure" $d^4$ ground state, $[Mn(III)I^-]^{2+}$ ($d^1_{xy}d^1_{yz}d^1_{xz}d^1_{z^2}5p^6$), that corresponds to $^5B_1 \otimes {}^1S$. Use of a valence bond configuration interaction model (VBCI) that includes the 29 basis functions from $^4B_1 \otimes {}^2P$ (24) and $^5B_1 \otimes {}^1S$ (5) combined with estimates as to the ranges of relevant energy levels leads to a calculation of positive value for $D$ between 0.2 and $10\,cm^{-1}$—much better agreement with experiment than what would be obtained from the pure $d^4$ model. The qualitative message from this study is that transition metal ions with heavy elements as ligands (e.g., iodine) can lead to anomalous results for zfs, due to combination of LMCT (giving spin on these ligands) and the large SOC for heavy elements (giving large magnitude contributions to zfs).

Given that among all of the integer-spin transition metal systems studied thus far by HFEPR, Mn(III) has proven the most successful it is not surprising that the highest accuracy HFEPR data have been obtained for this ion. An $S = 2$ system, such as Mn(III) can have fourth order terms in the spin Hamiltonian, but these are difficult to determine without single-crystal data, which provides the necessary narrow linewidths. The pioneering study by Gerritsen and Sabisky was of a single crystal and they were able to determine a fourth order zfs [53]. Much more recently, Mossin et al. performed a single crystal W-band study of $[Mn(cyclam)Br_2]Br$ and were able to extract fourth-rank terms [64]; such terms were also extracted for alum crystals containing $[Mn(H_2O)_6]^{3+}$ [58], as mentioned above. However, we recently found it possible to determine fourth-rank zfs terms from HFEPR spectra of a pure polycrystalline powder of $[Mn(dbm)_2(py)_2](ClO_4)$ [56]. This was possible due to a complete lack of field-induced orientation effects, and the consequent nearly perfect agreement of the experimental spectra with powder pattern simulations (Fig. 3). The complete set of spin Hamiltonian parameters for this complex are: $D = -4.504(2)$, $E = -0.425(1)$, $B_4^0 = -1.8(4) \times 10^{-4}$, $B_4^2 = 7(3) \times 10^{-4}$, $B_4^4 = 48(4) \times 10^{-4}\,cm^{-1}$, $g_x = 1.993(1)$, $g_y = 1.994(1)$, $g_z = 1.983(1)$. Although the determination of fourth-rank zfs parameters could be considered an academic exercise, these terms of the spin Hamiltonian may be significant in specific cases, as in high-spin molecular clusters, where they were proposed to influence quantum tunneling probability between the particular $\pm M_S$ states through breaking the symmetry of the zfs tensor [12].

### 3.6. Mn(II) ($d^5$, $S = 5/2$)

The ground-state electronic term for the free ion of this oxidation state of manganese is $^6S$. This spherically symmetric term is unaffected by a ligand/crystal field and is thus a $^6A_{1g}$ term in octahedral symmetry. Zfs arises only from higher order mixing in of lower spin excited states [65,66] and is generally small ($<1\,cm^{-1}$). A vast number of EPR studies have been performed on octahedral Mn(II) and we refer only to Abragam and Bleaney [1]. HFEPR can, however, be useful when the Mn(II) ion is

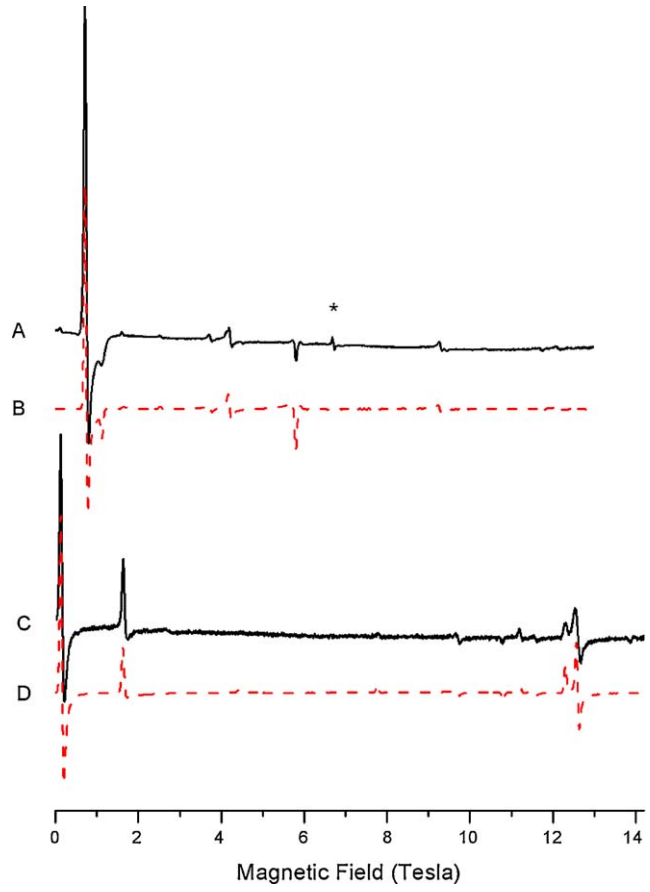


Fig. 3. An example of (nearly) perfect powder HFEPR spectra of an $S=2$ system: polycrystalline $[Mn(dbm)_2(py)_2](ClO_4)$ at 40 K. Solid lines: experiments at 187.51 GHz (A) and 438.15 GHz (C); dotted lines: simulations at the same conditions. Spectra (B) and (D) were simulated using spin Hamiltonian parameters as in text and in Table 1. The line marked with an asterisk originates from a Mn(II) impurity and is not reproduced in the simulations.

found in highly distorted octahedral or tetrahedral symmetry. Freed and co-workers have made several such studies [67–71]. A class of Mn(II) complexes quite similar to those mentioned above for V(II) and Cr(III) has been investigated by HFEPR at 249 GHz, namely, $[MnL_4X_2$ or $Mn(L–L)_2X_2]$, where L = γ-picoline, L–L = *o*-phenanthroline; X = Cl, Br, I [67]. Lynch et al. found that the value of $D$ increased steadily with larger halo ligand, e.g., for L = γ-picoline: $D = 0.186$, 0.626 and 0.999 $cm^{-1}$, respectively, for X = Cl, Br, I [67]. These workers also studied Mn(II) protoporphyrin IX and obtained $D = 0.775\,cm^{-1}$, $|E/D| = 0.048$. Their use of high frequency (249 GHz) and magnetic fields up to 9.5 T allowed determination of zfs parameters with much greater accuracy for this biologically important complex than had been previously possible with use of conventional X- and Q-band EPR [72]. This square planar protoporphyrin IX complex represents an upper limit of $|D|$ in Mn(II) with only light atoms as ligands. Tetrahedral Mn(II) complexes of general formula $[Mn(OPPh_3)_2X_2]$, where X = Cl, Br, I, have also been studied by HFEPR [68]. Again, there is a steady increase in zfs with larger halo ligand: $D = 0.165$, 0.507 and 0.906 $cm^{-1}$, respectively, for X = Cl, Br, I, with $E/D$ roughly constant (∼0.260(15)) [68].

A very thorough study of an extensive series of five-coordinate Mn(II) complexes has very recently been reported by Mantel et al. [73]. These complexes are of general formula $[Mn(terpy)X_2]$ (X = Cl, Br, SCN), similar to those mentioned above for Mn(III). This study is particularly interesting in that for two of the complexes, the zfs is positive ($D = +1.000$, $+0.605\,cm^{-1}$, respectively, for X = I, Br), but for the other two it is negative: ($D = -0.26$, $-0.30\,cm^{-1}$, respectively, for X = Cl, SCN) [73]. This result clearly demonstrates both the importance of SOC contributions from coordinating ligands (as described above for $Mn(cyclam)I_2$ [63]) and the difficulty of using the sign or the magnitude of $D$ in complexes of Mn(II) for structural correlations. It also should be noted that HFEPR allows very accurate determination of the intrinsic $g$ values for Mn(II), but these values are always very close to 2.00 and are generally uninformative.

A final, and very important application of HFEPR of Mn(II) is in authentic metalloproteins [74–77]. Specific examples are Mn lipoxygenase, studied at W-band by Gaffney et al. [74], and MnSOD in its Mn(II) state, studied by Un and co-workers [75–77]. Frequencies of 190 and 285 GHz were employed and the zfs parameters were determined in the latter series of papers for a range of MnSOD enzymes from different organisms and different site-directed mutants. The sensitivity of HFEPR to slight changes in zfs among these metalloproteins ($|D|$ ranged from 0.35 to 0.36 $cm^{-1}$, although $|E/D|$ showed much greater variation, ranging from 0.02 to 0.09 [76]) allowed distinguishing amongst them and making possible structural/functional correlations [77]. A general result of this work is that the low symmetry sites that occur in metalloproteins lead to relatively high zfs for Mn(II) thus making HFEPR investigations both feasible and useful.

### 3.7. Fe(III) ($d^5$, $S = 5/2$)

Fe(III) is isoelectronic with Mn(II), yet there are many crucial differences. The higher charge for a 3+ versus 2+ ion, combined with the greater covalency for Fe versus Mn leads to far more LS compounds of Fe(III) as opposed to Mn(II). Nevertheless, there is a large number of HS complexes of Fe(III), including many of biological importance, such as heme proteins with weak axial ligands such as aqua or fluoro, and many non-heme Fe enzymes (which can also be found in oxidation and spin states other than HS Fe(III)). Despite this enormous biological importance of Fe(III) and its plethora of coordination complexes and materials applications, HFEPR, as opposed to conventional EPR, has been relatively little applied to this system.

Fe(III) in an axial environment, such as HS ferric heme proteins, is generally characterized by very large zfs. Correspondingly, it exhibits conventional EPR resonances for $S = 5/2$ in the low-field limit, $g\beta H \ll D$, and as a result signals with effective $g_\perp = 6$ and $g_{||} = 2$ are observed [1,78]. Such signals are qualitatively useful, but not quantitatively so, except in showing whether slight rhombicity occurs. Gaffney and co-workers provide a recent example of a very comprehensive study of an interesting ferric heme protein, coral allene oxide synthase [79]. For the purposes here, we simply note that W-band (94 GHz)

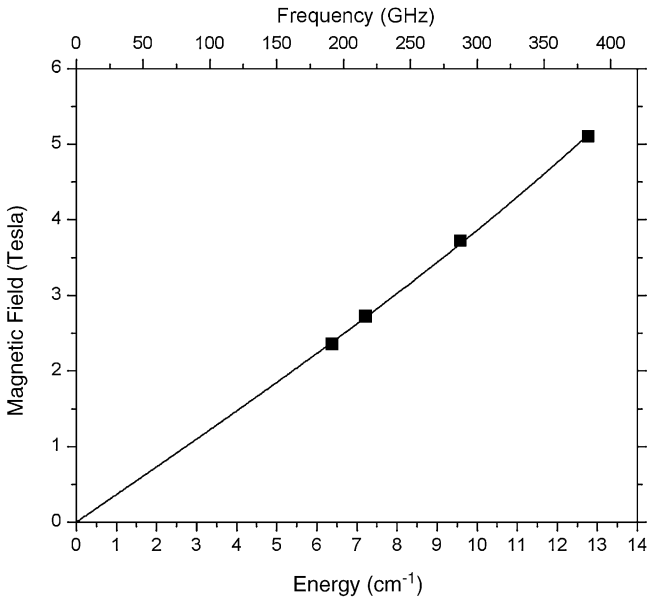


Fig. 4. Determination of spin Hamiltonian parameters for $S = 5/2$ from the "curving" of the perpendicular intra-Kramers $M_S = \pm 1/2 \leftrightarrow \mp 1/2$ turning point: HFEPR at 4.5 K on horse heart met-myoglobin (sample volume, 280 μL; protein concentration, 10 mM; buffer, 200 mM phosphate pH 7). The squares are experimental resonances, while the best-fit line was drawn using: $D = 10.1\ \mathrm{cm}^{-1}$, $g_\perp = 1.96$ [82].

EPR provided (effective) $g_x$ and $g_y$ values that were not measurably different from those at X-band [79], which results from the zfs being in the range 5–10 $\mathrm{cm}^{-1}$. In theory, microwave quanta larger than that at W-band might allow observation of resonances other than simply the $M_S = \pm 1/2 \leftrightarrow \mp 1/2$ transition, observable at low frequencies. As shown by Alpert et al. [16], this is not the case for met-hemoglobin (Fe(III) hemoglobin with axial aqua ligands). This work was possibly the first HFEPR experiment on a HS metal ion, and deserves credit for introducing the multifrequency methodology using tunable sources (BWOs) at this very early (1973!) stage. The authors observed that the perpendicular turning point of the allowed $M_S = \pm 1/2 \leftrightarrow \mp 1/2$ transition in an $S = 5/2$ system is "curving" when observed over a wide enough frequency range (in their case, 75–430 GHz) (for an analogous experiment, see Fig. 4). In other words, $g_{\mathrm{eff}}$ changes from approximately $g_\perp = 6$ to smaller values with increasing frequency, and this frequency dependence allows one to calculate the axial parameter $D$, in their case estimated as $10.7(2)\ \mathrm{cm}^{-1}$ with (intrinsic) $g_\perp = 1.95(1)$. This remarkable work was extended much more recently by van Kan et al. [80] who studied met-myoglobin by multifrequency EPR between 1 and 285 GHz. Although the curving of the $g_\perp$ transition has been confirmed, the extraction of the relevant spin Hamiltonian parameters from it was difficult due to line broadening at high frequencies, attributed to $D$-strain. The final estimates were: $D = 9.0$–$9.5\ \mathrm{cm}^{-1}$ and (intrinsic) $g_\perp = 1.98$. The merits of observing the curving of the perpendicular $M_S = \pm 1/2 \leftrightarrow \mp 1/2$ turning point in HS Fe(III) spectra with increasing frequency are further discussed in the review by Andersson et al. [81]. For example, the value for $D$ decreases from 9.5 to $5\ \mathrm{cm}^{-1}$ upon binding of fluoride ion to Fe(III) in met-myoglobin. Two methods of simulating the frequency dependence of the $g_{\mathrm{eff}\perp}$ are discussed based on the same example: third-order perturbation theory, and full matrix diagonalization of the spin Hamiltonian.

Finally, although the above described method of extracting zfs parameters from HS Fe(III) spectra in case of $D > g\beta H$ appears to be working reasonably well, some of us have recently observed for the first time the inter-Kramers transitions in a heme-related molecule [83]. The system in question was β-hematin or [Fe(III)-protoporphyrin-IX]$_2$, the synthetic equivalent of the malaria pigment hemozoin [84], and multifrequency EPR experiments were carried out in the frequency range of 9–500 GHz. The curving of the perpendicular $M_S = \pm 1/2 \leftrightarrow \mp 1/2$ turning point yields $D = 5.5\ \mathrm{cm}^{-1}$, while the inclusion of the inter-Kramers transition $M_S = \pm 1/2 \leftrightarrow \pm 3/2$ increases the accuracy of the spin Hamiltonian parameters, and yields $D = 5.85(5)\ \mathrm{cm}^{-1}$ and $g_\perp = 1.95(2)$. It thus appears that it is in principle possible to directly determine the zfs of HS ferric hemes from a full set of allowed transitions, including inter-Kramers resonances, at the HFEPR frequencies currently in use as long as $|D| \leq 10\ \mathrm{cm}^{-1}$.

In this context it is worth noticing that over thirty years ago, Richards and coworkers were able to directly measure zfs in HS Fe(III) porphyrins in both model compounds and proteins in a wider range of $D$ values by use of far-IR spectroscopy [85,86]. This truly landmark study provides information on zfs in HS Fe(III) that has not been matched even today. Among the complexes studied were polycrystalline dimethyl esters of protoporphyrin IX and deuteroporphyrin IX equatorially coordinating Fe(III) with a series of axial ligands: F, Cl, Br, I, and $N_3$ (for protoporphyrin IX, Br and I were not studied) The $D$ values in these cases ranged from 5 to $16\ \mathrm{cm}^{-1}$, and the measurement accuracy was in the range 0.1–$0.2\ \mathrm{cm}^{-1}$. Even more impressive is that met-myoglobin and its fluoro analogue and fluoro-met-hemoglobin were also studied in frozen aqueous solution and despite the relatively low concentration, accurate (down to ca. $\pm 0.1\ \mathrm{cm}^{-1}$) $D$ values were determined for these metalloprotein systems [86].

Fe(III) in other than the axial symmetry of porphyrins often exhibits an extremely rhombic EPR spectrum, exemplified by the effective $g = 4.3$ signal seen in conventional EPR. The EPR in this case was described in a landmark study by Aasa [87], who employed X- and Q-band EPR to determine $D = 0.84\ \mathrm{cm}^{-1}$ for Fe(III)-EDTA, which likely represents the uppermost value of $D$ than can be measured for $S = 5/2$ with use of conventional EPR. As shown by Renault et al. [88], it is possible to employ X-band EPR of this signal and extract a wealth of information on the electronic structure, in their case of FeSOD, the Fe(III) analogue to MnSOD mentioned above. Variable temperature X-band EPR studies of the transitions which arise from different $M_S$ manifolds allowed an estimate of $D = -2\ \mathrm{cm}^{-1}$ [88]. HFEPR studies of non-heme HS Fe(III) are relatively rare, especially compared to Mn(II). A prime example is the recent work of Meštric et al. on a ferric impurity center in the ferroelectric phase of $PbTiO_3$ [89]. While X-band EPR displays the usual uninformative $g_\perp \sim 6$ and $g_{||} \sim 2$ resonances, HFEPR performed at 95 and 190 GHz delivered accurate values of the relevant spin Hamiltonian parameters: $D = 1.1760(3)\ \mathrm{cm}^{-1}$ and $g_{\mathrm{iso}} = 2.002$. Further

examples are studies of Fe(III) dopants in solid state materials: a pigment based on corundum and hercynite ($FeAl_2O_4$) [90], zeolites [91], and alumina [92]. In the pigment, X-band EPR is difficult to interpret on its own, but 95 GHz EPR allows straightforward determination of a nearly axial $D = 0.185\,cm^{-1}$ (thus comparable in magnitude to the X-band quantum). However, in the zeolite, the zfs for Fe(III) is much smaller ($D \sim 0.1\,cm^{-1}$, comparable to that in many cases for Mn(II)), thus the use of HFEPR (up to 475 GHz) in such a case is a luxury. In the case of the alumina dopants, HFEPR (at 130 GHz, along with X- and Q-band data) was crucial in the very elegant determination of higher order terms in the spin Hamiltonian for Fe(III) ($B_4^0$, $B_4^3$ parameters) [92]. The $D$ value in this case was on the low side of typical non-heme HS Fe(III) values, equal to $0.1683\,cm^{-1}$, while $B_4^0 = -1.8 \times 10^{-4}$ and $B_4^3 = 36 \times 10^{-4}\,cm^{-1}$.

Once again, however, the work of Brackett et al. set the standard for six-coordinate Fe(III) wherein they studied a series of Fe(III) dithiocarbamates, $[Fe(R_2NCS_2)_2]X$, where X = Cl, Br, R = methyl, ethyl, iso-propyl [86]. These complexes, studied as polycrystalline solids, but also in one case as a single crystal, exhibit intermediate spin, $S = 3/2$, and large and widely ranging zfs, $4 \leq D \leq 17\,cm^{-1}$.

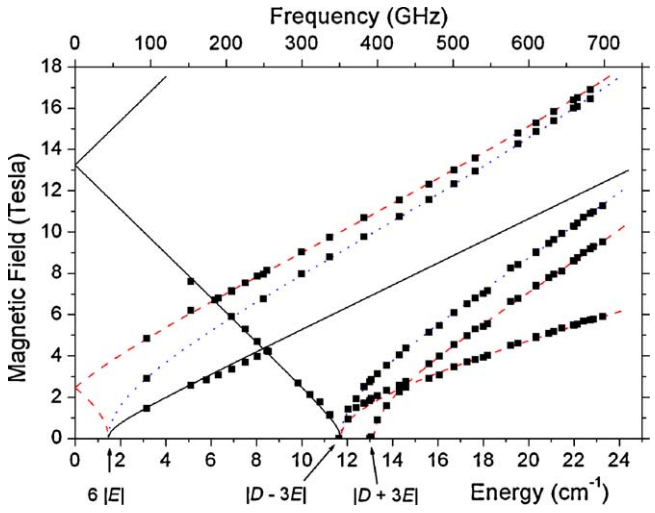


Fig. 5. Tunable-frequency EPR in an $S = 2$ system. Resonance field vs. sub-THz wave quantum energy dependence for EPR transitions in polycrystalline $[Fe(btz)_2(SCN)_2]$. Experimental points are represented by squares. Simulations using spin Hamiltonian parameters as in text and Table 1 are shown by dashed lines for $x$ turning points, dotted lines for $y$ turning points, and solid lines for $z$ turning points. Three zero-field resonances, of which two are directly detectable in the 95–700 GHz range, are labeled accordingly.

### 3.8. Fe(II) ($d^6$, $S = 2$)

Among all of the integer-spin transition metal ions, high-spin Fe(II) is clearly that with the greatest relevance to bioinorganic chemistry, in coordination numbers ranging from three to six. We will discuss here only four- and six-coordinate complexes of Fe(II). The ground-state electronic term for the free ion of this oxidation state of iron is $^5D$. An octahedral crystal/ligand field splits this term into a high-lying orbital doublet $^5E_g$ and a low-lying orbital triplet $^5T_{2g}$. In the case of a truly octahedral system, a single resonance is observable at X-band at an effective $g$ value of ~3.4–3.6 [1]. However, in most complexes, the symmetry is lower and a variety of orbital ground states are possible (e.g., $^5A_1$ or $^5B_2$), depending on the type of distortion [8,93].

Despite the large number of six-coordinate Fe(II) complexes in existence, this system has proven very difficult to study by HFEPR with only a few such examples reported. One such study was of the complex $[Fe(Im)_6](NO_3)_2$ [8]. However, the main thrust of this work was INS investigations, which directly gave the energy levels of the ground-state spin quintet. Very few HFEPR transitions were observed and the signal/noise ratio was poor. Subsequently, we investigated by HFEPR a different, lower-symmetry six-coordinate Fe(II) complex, $[Fe(btz)_2(SCN)_2]$, and a wealth of transitions were observed that yielded the following set of spin Hamiltonian parameters: $D = +12.418(12)\,cm^{-1}$, $E = +0.243(3)\,cm^{-1}$; $g_x = 2.147(3)$, $g_y = 2.166(3)$, $g_z = 2.01(1)$ (Fig. 5) [94]. $[Fe(btz)_2(SCN)_2]$ is of interest for its relation to spin crossover systems and could be considered as having some relation to the active site of non-heme Fe enzymes; however, it is a relatively elaborate heteroleptic complex. It would be desirable to obtain HFEPR spectra of relatively simple (homoleptic) six-coordinate Fe(II) complexes to build a database of this important transition metal system. Such was among the goals of the study on $[Fe(Im)_6]^{2+}$ [8]; however, the HFEPR spectra were less than ideal.

Very recently, we have performed HFEPR (and parallel FDMRS) studies on two hexaaqua complexes of Fe(II): $[Fe(H_2O)_6](ClO_4)_2$ and $(NH_4)_2[Fe(H_2O)_6](SO_4)_2$, historically known as ferrous ammonium sulfate [93]. Studies were also performed on ferrous sulfate heptahydrate, however the results were unreliable due to heterogeneity in the sample, which was the consequence of the facile loss of hydration water. The results for $[Fe(H_2O)_6](ClO_4)_2$ were the most rewarding and could be combined with previous FDMRS data on $[Fe(H_2O)_6](SiF_6)_2$ [95]. This combination thus provided a reference point in spin Hamiltonian parameters for $[Fe(H_2O)_6]^{2+}$: $D = 11.5(3)\,cm^{-1}$, $E = 0.7(1)\,cm^{-1}$.

We next discuss four-coordinate complexes. A tetrahedral crystal/ligand field splits the $^5D$ free-ion term into a high-lying orbital triplet $^5T_2$, and a low-lying doublet triplet $^5E$. In this case, distortions from $T_d$ symmetry, such as a compression/elongation along a $C_2$ axis breaks the degeneracy of the $^5E$ ground state to, respectively, give a $^5A_1$ or $^5B_1$ ground state. The situation for tetrahedral $d^6$ is of course analogous to that for octahedral $d^4$, as described above for Cr(II).

A very significant tetrahedral Fe(II) complex has been studied by HFEPR: $(PPh_4)_2[Fe(SPh)_4]$, which is a model for the reduced form of the active site of the iron–sulfur protein, rubredoxin ($Rd_{red}$) that comprises an Fe ion coordinated by four cysteine thiolate residues [96]. HFEPR studies of this complex in the solid state yielded the following spin Hamiltonian parameters: $D = +5.84\,cm^{-1}$, $E = +1.42\,cm^{-1}$, $g_x = g_y = 2.08$, $g_z = 2.00$ [96]. The positive sign for $D$ is as expected for tetragonal compression, as is indicated from the crystal structure of the complex. An important aspect of this study is that, as is the case in principle for all Fe complexes, the data can be compared to that

obtained from Mössbauer effect spectroscopy. Mössbauer studies suggested that $D = +7.6\,cm^{-1}$, $E = 2.1\,cm^{-1}$, which values are quite different from those obtained by fits of the 2D resonant field-frequency dataset from HFEPR [96]. Thus, although Mössbauer effect spectroscopy is an extremely powerful technique for the study of Fe complexes, particularly in biological systems [97], compared to HFEPR or FDMRS, it is not necessarily ideal for determination of electronic spin Hamiltonian parameters. However, a pioneering study employing FDMRS on the same complex gave $D = +5.98\,cm^{-1}$, $E = +1.42\,cm^{-1}$ [95], in excellent agreement with the HFEPR results. FDMRS has also recently been applied to a bis(benzene-1,2-dithiolato) complex of (formally) Fe(II) with an intermediate spin ($S = 1$) ground state with very large zfs ($+28\,cm^{-1}$), out of the range of HFEPR [98].

### 3.9. Co(II) ($d^7$, $S = 3/2$)

The ground-state electronic term for the free ion of this oxidation state of cobalt is $^4F$. An octahedral crystal/ligand yields the (orbital triplet) ground $^4T_{1g}$ state while a tetrahedral crystal/ligand yields the ground (orbital singlet) $^4A_2$ state, which is suitable for HFEPR investigation. SOC in the conditions of lower than cubic symmetry splits each of these spin-quartet states into two Kramers doublets, the energy difference between them being the zfs. Co(II) is thus generally EPR-active at conventional frequencies and fields; however, conventional EPR spectra are uninformative with respect to zfs. Simple ligand-field considerations indicate that the two general classes of HS Co(II) coordination complexes (six- and four-coordinate) differ greatly in the magnitude of zfs. Octahedral complexes are characterized by very large $D$, of the order of $100\,cm^{-1}$ [6]. This magnitude of zfs cannot be measured by HFEPR; the information is thus obtained by other methods, notably magnetometry. Tetrahedral Co(II) complexes, on the other hand, generally have smaller zfs. Its magnitude has been a bone of contention for a long time, with different (indirect) techniques such as conventional EPR or MCD yielding different values of $D$ [7]. Even the sign of $D$ could not normally be unequivocally established [99,100].

The moderate magnitude of zfs in tetrahedral Co(II) complexes makes them amenable to HFEPR experiments. The first such experiment was reported by van Stapele et al. on the $[CoX_4]^{2-}$ ion contained in single crystals of the $Cs_3CoX_5$ salts (X = Cl, Br) [101]. HFEPR performed at frequencies of 70–72 and 110–120 GHz, with magnetic fields up to 9 T delivered by a pulsed magnet, resulted in a direct measurement of spin Hamiltonian parameters, which were found to be: $D = -4.30(4)\,cm^{-1}$, $E = 0$, $g_\perp = 2.30(2)$, $g_{||} = 2.40(2)$ for $Cs_3CoCl_5$ and $D = -5.34(10)\,cm^{-1}$, $E = 0$, $g_\perp = 2.32$, $g_{||} = 2.42$ for $Cs_3CoBr_5$.

Progress in instrumentation has made possible a tunable-frequency HFEPR experiment on another pseudo-tetrahedral HS Co(II) complex, $Co(PPh_3)_2Cl_2$ [102]. Frequencies in the 150–700 GHz range in conjunction with magnetic fields up to 25 T enabled us to directly measure spin Hamiltonian parameters of the ground state for this complex, which were found to be: $D = -14.76(2)\,cm^{-1}$, $E = -1.141(8)\,cm^{-1}$, $g_x = 2.166(4)$, $g_y = 2.170(4)$, $g_z = 2.240(5)$ (Fig. 6). This experiment proved that it is possible to measure very accurately *intrinsic* (as opposed to effective) spin Hamiltonian parameters for tetrahedral HS Co(II) characterized by $|D|$ of the order of $15\,cm^{-1}$ and higher. Another important aspect of this study was that VTVH–MCD measurements on powder $Co(PPh_3)_2Cl_2$ gave essentially the same zfs values as did HFEPR, thus validating the use of VTVH–MCD for this application. A study of a larger number of tetrahedral Co(II) complexes coordinated with a series of scorpionate (trispyrazolylborate) ligands has shown that the zfs can differ over a wide range, with $|D|$ varying from ca. 2 to $20\,cm^{-1}$ [20].

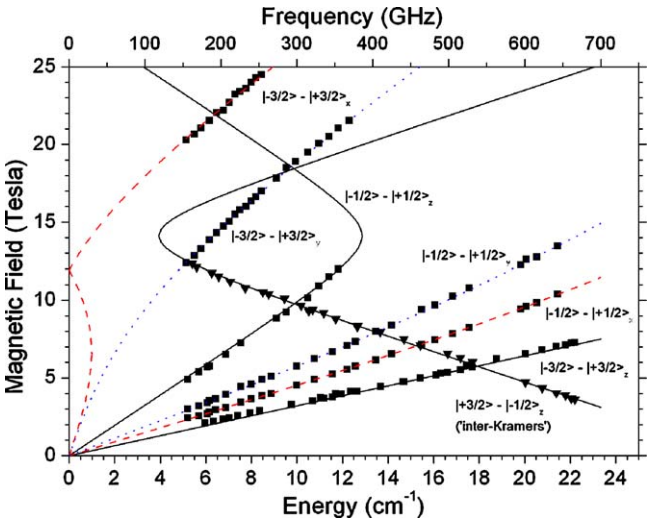


Fig. 6. Tunable-frequency EPR in an $S = 3/2$ system. Resonance field vs. sub-THz quantum energy dependence for EPR transitions in polycrystalline $CoCl_2(PPh_3)_2$. The squares represent experimental intra-Kramers resonances while the triangles denote an inter-Kramers turning point branch. Simulations using the spin Hamiltonian parameters as in text, and in Table 1 are shown by dashed lines for $x$ turning points, dotted lines for $y$ turning points, and solid lines for $z$ turning points. Particular transition branches are identified and labeled accordingly. The only zf resonance appears outside the experimental range at ca. 900 GHz, but the $M_S = -1/2 \leftrightarrow +3/2$ inter-Kramers turning point branch leading to it (marked by triangles) yields a very accurate estimate of the zfs.

### 3.10. Co(I) ($d^8$, $S = 1$) and Co(III) ($d^6$, $S = 1$–2)

Co(I), a rather rare but stable oxidation state of cobalt, is isoelectronic with Ni(II) (see Section 3.11 below). We are not aware of attempts to use HFEPR in order to determine the zfs in any coordination complex of this particular ion other than our own preliminary results on a series of complexes $Co(PPh_3)_3X$ (X = Cl, Br) [103]. For the Cl complex, the approximate zfs parameters are the following: $|D| = 5.4\,cm^{-1}$, $|E| = 0.4\,cm^{-1}$, while those for the Br complex are of much smaller magnitude: $|D| = 2.5\,cm^{-1}$, $|E| = 0.25\,cm^{-1}$. The same trend was previously observed for the analogous series of Ni(II) complexes [104]. In both cases $g$ is approximately isotropic and equal to ~2.2, which is again a value close to that for the Ni(II) complexes. A detailed spectral analysis of the Co(I) series as well as its interpretation is pending.

Lastly, we note that Ray et al. [98] studied a formally Co(III) dithiolato complex, which also has an $S = 1$ ground state and a

zfs of +32 $cm^{-1}$ as determined by FDMRS. However, in this complex the ligands are very non-innocent (i.e., of extensive S-based radical character, as opposed to thiolate anion) and the cobalt ion cannot be easily classified as either Co(III) or Co(II). We have performed HFEPR studies on the only authentic HS complex of Co(III), $[CoF_6]^{3-}$ (as its $K_3$ salt); the spectra are indicative of a non-Kramers HS system, but have not yet been fully analyzed [105].

### 3.11. Ni(II) ($d^8$, $S = 1$)

The ground-state electronic term for the free Ni(II) ion is $^3F$. An octahedral crystal/ligand field yields the ground orbital singlet $^3A_{2g}$, while a tetrahedral crystal/ligand field yields the ground orbital triplet $^3T_1$. However, the symmetry is lower in most tetrahedral complexes, which have generic formulas $[NiL_2X_2]$ ($C_{2v}$ symmetry) or $[NiY_3X]$ ($C_{3v}$ symmetry). In both cases, the ground state is an orbital singlet, $^3B_1$ or $^3A_2$, respectively, which greatly facilitates employment of HFEPR.

HFEPR studies have been performed on a variety of octahedral complexes of Ni(II). The first example of such known to us is the very early (1953) study by Ono on the hexaaqua $Ni^{2+}$ ion contained in crystalline nickel sulfate heptahydrate ($NiSO_4{\cdot}7H_2O$), representing the $O_6$ coordination sphere [106]. Using frequencies of 44 and 55 GHz produced by a very rudimentary device (a magnetron harmonic generator), Ono was able to measure the zfs parameters of this species as $D = -3.5\ cm^{-1}$ and $E = -1.5\ cm^{-1}$. The following examples of HFEPR experiments on octahedral Ni(II) complexes include a complex with $N_6$ donor sets [107–109], with an $O_4N_2$ donor set [110], with an $O_2N_4$ donor set [107], and with a more complex ligand donor set in the complex $Ni(hmp)_4(dmb)_4Cl_4$ embedded in its diamagnetic host equivalent containing the Zn ion [111]. In most of these cases, the zfs is relatively small, e.g., $D = +1.44\ cm^{-1}$ [109] (see also Table 1), although the complex measured by Yang et al. displays a much larger magnitude of zfs: $D = -5.35(5)$ and $E = \pm 1.20(2)\ cm^{-1}$ [111]. The appearance of octahedral Ni(II) spectra is often similar to that observed for optically excited aromatic triplets, such as those studied many years ago [112,113], the only difference being that the zfs parameters, and consequently frequencies and resonant magnetic fields are approximately one order of magnitude larger for Ni(II) than for classical aromatic hydrocarbon systems. A notable exception to this rule is the complex $[Ni\text{-}(HIM2\text{-}py)_2NO_3]NO_3$, as reported by Rogez et al. [114]. Due to a highly distorted geometry the zfs is large, comparable to tetrahedral Ni(II) complexes (see below). A combination of different experimental techniques was employed, including HFEPR and FDMRS. $D$ was found to be negative and equal to $-10.15\ cm^{-1}$ (HFEPR) or $-10.1(1)\ cm^{-1}$ (FDMRS), with a small rhombic factor $E/|D| = 0.01$ (HFEPR) or 0.02 (FDMRS), and $g_{iso} = 2.17$.

Significantly larger zfs occurs for tetrahedral than octahedral complexes. Some of us have studied the series $[Ni(PPh_3)_2X_2]$ (X = Cl, Br, I) by HFEPR over the frequency range 90–550 GHz [104] and found the following parameters for the chloro complex: $D = +13.196(2)\ cm^{-1}$, $E = +1.848(6)$, $g_x = 2.200(5)$, $g_y = 2.177(1)$, $g_z = 2.15(1)$ [20]. These parameters represent the latest available data for this complex using tunable-frequency HFEPR, and differ slightly from those reported earlier [104], which were based on a multifrequency experiment. These results, in combination with an earlier single-crystal electronic absorption study allowed a complete description of the electronic structure of Ni(II) in this complex. The HFEPR results for the chloro complex were subsequently confirmed by FDMRS [115]. The results for X = Br and I were more ambiguous. For the bromo complex, there was the complication of two crystalline forms, and for the iodo complex, the zfs was too large to be measurable by HFEPR ($|D|$ estimated at $23\ cm^{-1}$ by magnetometry). Qualitatively, the last result shows again the difficulties associated with coordination by heavy atom ligands, in this case leading to very large zfs as apparently the contribution from SOC on I adds to that from Ni(II), as opposed to subtracting as in the case described above for Mn(III) [63].

### 3.12. Rare earth (f block) ions

The f block ions are very often found in paramagnetic ground states, but represent a complicated situation for magnetic resonance due to their extensive contributions from orbital angular momentum, so that $J$ ($J = |L - S|, \ldots, |L + S|$) rather than $S$ is a good quantum number [1]. An exception, for which the standard spin Hamiltonian readily applies, is the half-filled electronic configuration $f^7$, best exemplified by Gd(III). The situation is similar to that for Mn(II) and the zfs in Gd(III) is typically in the same range as that found in Mn(II) complexes, i.e., $D \ll 1\ cm^{-1}$. Zfs of this order of magnitude makes conventional (X-band) EPR spectra, although readily detectable [1], often difficult to interpret, particularly in the case of powder patterns. Examples of several coordination complexes of Gd(III) can be found, e.g., in [116]. For the classical complex $Gd(acac)_3$, $D$ was estimated as $0.073\ cm^{-1}$, although the spectra simulated using this parameter were not presented, so the agreement between experiment and simulation could not be evaluated. In view of the difficulties with spectral interpretation, it is often practical to move to higher frequencies, i.e., apply HFEPR, so that the Zeeman term of the spin Hamiltonian dominates over zfs, similarly to what is done with Mn(II) and non-heme HS Fe(III).

An example of the application of HFEPR to study Gd(III) is the multifrequency (9, 35 and 130 GHz) study by Priem et al. of Gd(III) sites in α-alumina ($Al_2O_3$) [92]. This approach together with a very careful spectral analysis allowed them to determine not only the second-rank zfs axial parameter $3B_2^0 (\equiv D) = 0.1033\ cm^{-1}$, but also fourth-rank parameters $B_4^0$ and $B_4^3$, and even sixth-rank spin Hamiltonian terms $B_6^0$ and $B_6^6$. In particular, it was found that while high frequencies help to estimate the even terms $B_n^i$ ($n = 2, 4$; $i = 2, 4, 6$), low frequencies are more helpful to determine the odd term $B_4^3$.

Finally, zfs in Gd(III) in liquid solution (as opposed to solids discussed for the most part in this review), have also been measured by multifrequency EPR, including HFEPR at 94 and 249 GHz by Clarkson et al. [117] in the form of MRI contrast agents DTPA and DOTA chelates. In a liquid, zfs is typically averaged by the rapid tumbling motion of the molecules to yield

a single, uninformative resonance near $g = 2$. However, the multifrequency approach allowed the authors of the quoted paper to obtain the parameter $\Delta^2 = D_{xx}^2 + D_{yy}^2 + D_{zz}^2$, where $D_{ii}$ are the diagonal elements of the time-dependent zfs tensor, from the frequency dependence of the $g_{\text{eff}}$ of the single observed resonance line, analogously to the procedure discussed for HS Fe(III) in Section 3.7. The values obtained are of the same order of magnitude as in other Gd(III) complexes measured in solid form, i.e., $\sim 0.1\,\text{cm}^{-1}$.

Although $S$ is normally not a good quantum number for most f-block ions, Ho(III) ($f^{10}$) behaves like a non-Kramers ion and can be described by the term $^5I_8$. It was investigated as a dopant in the cubic double fluorite crystal $KY_3F_{10}$ by Tarasov et al. [42]. Low-symmetry crystal field gives rise to significant zfs, of the order of $\sim 5.8\,\text{cm}^{-1}$ as determined by tunable-frequency EPR at conventional fields.

## 4. Conclusions

Over a relatively brief time, less than a decade, HFEPR has become a powerful tool in the spectroscopic investigation of coordination complexes of paramagnetic transition metal ions that had not been amenable to study by conventional EPR (frequencies up to 35 GHz, magnetic fields up to 2 T). HFEPR studies have been performed on complexes of nearly all high-spin first row transition metal ions, most notably Mn(III), but many others as well. Advances in instrumentation, such as the use of tunable, or quasi-tunable frequency sources, quasi-optical propagation techniques, ever higher fields, and developments in fitting and analytical software have contributed greatly to these advances. Fitting of dense HFEPR field-frequency datasets allows determination of spin Hamiltonian parameters with tremendous precision (in ideal cases $D$, $E$ values better than $\pm 0.001\,\text{cm}^{-1}$, and quite routinely $\pm 0.01\,\text{cm}^{-1}$), significantly greater than that obtainable from magnetometry. More important is that HFEPR, as a resonance technique, provides much greater accuracy in determining all of the spin Hamiltonian parameters (especially the $E$ term, and potentially fourth-order terms) than magnetometry, and in the case of Fe, from Mössbauer effect spectroscopy. Many of these recent HFEPR studies have applied ligand-field theory to make full use of these parameters to understand the complete electronic structure of these transition metal ion complexes.

Nevertheless, there are many needs and opportunities for further applications of HFEPR in coordination chemistry, particularly in biological applications. Thus far, only Mn(II), which is a Kramers system and has relatively small zfs, as expected for a $d^5$ system, has been fruitfully investigated by HFEPR in an authentic metalloenzyme system so that zfs parameters were directly extracted [75,76]. HFEPR has also been performed on high-spin Fe(III) in a metalloprotein [16,80]. In principle, there are many metalloproteins that contain high-spin transition metal ions, including Kramers ions such as Fe(III) and non-Kramers ions such as Fe(II), both as found in mononuclear sites such as in non-heme Fe proteins, rubredoxins and related systems, and in polynuclear sites such as in FeS proteins. Fe(IV), with $S = 1$, is also involved in metallobiochemistry. Metalloproteins containing Mn, Ni, and Co, and other potentially high-spin transition metal ions are continually being discovered, opening new potential applications for HFEPR.

## Acknowledgements

This work was supported by the National High Magnetic Field Laboratory, which is funded by the NSF through Cooperative Agreement DMR 0084173, and the State of Florida, and by the Roosevelt University.

## References

[1] A. Abragam, B. Bleaney, Electron Paramagnetic Resonance of Transition Ions, Dover Publications, Inc., New York, 1986.
[2] F.A. Cotton, G. Wilkinson, P.G. Gaus, Basic Inorganic Chemistry, Wiley, New York, 1995, p. 514.
[3] For the purpose of this review, 'high frequency' means any frequency significantly above Q-band (35 GHz) and 'high field' means magnetic field above that obtainable with a conventional electromagnet (about 2 T).
[4] G.M. Smith, P.C. Riedi, in: B.C. Gilbert, M.J. Davies, D.M. Murphy (Eds.), Electron Paramagnetic Resonance, Royal Society of Chemistry, Cambridge, UK, 2002, p. 254.
[5] W. Hagen, Coord. Chem. Rev. 190 (1999) 209.
[6] R.L. Carlin, C.J. O'Connor, S.N. Bhatia, J. Am. Chem. Soc. 98 (1976) 685.
[7] J.A. Larrabee, C.M. Alessi, E.T. Asiedu, J.O. Cook, K.R. Hoerning, L.J. Klingler, G.S. Okin, S.G. Santee, T.L. Volkert, J. Am. Chem. Soc. 119 (1997) 4182.
[8] G. Carver, P.L.W. Tregenna-Piggott, A.-L. Barra, A. Neels, J.A. Stride, Inorg. Chem. 42 (2003) 5771.
[9] C. Dobe, C. Noble, G. Carver, P.L.W. Tregenna-Piggott, G.J. McIntyre, A.-L. Barra, A. Neels, S. Janssen, F. Juranyi, J. Am. Chem. Soc. 126 (2004) 16639.
[10] R. Boča, Coord. Chem. Rev. 248 (2004) 757.
[11] D. Gatteschi, L. Sorace, R. Sessoli, A.-L. Barra, Appl. Magn. Reson. 21 (2001) 299.
[12] A.-L. Barra, L.-C. Brunel, D. Gatteschi, L. Pardi, R. Sessoli, Acc. Chem. Res. 31 (1998) 460.
[13] Sometimes, yet a different set of zfs parameters is used, noted $b_p^q$. In this notation, $b_2^i = 3B_2^i (i = 0, 2)$; $b_4^i = 60B_4^i (i = 0, 2, 4 \text{ or } 0, 3, 6)$. In the rare cases this notation was used in the literature, we re-calculated the respective parameters into the $B_p^q$ format.
[14] M.J. Mombourquette, J.A. Weil, J. Magn. Reson. 99 (1992) 37.
[15] L.-C. Brunel, Appl. Magn. Reson. 3 (1992) 83.
[16] Y. Alpert, J. Couder, J. Tuchendler, H. Thome, Biochim. Biophys. Acta 332 (1973) 34.
[17] P.L.W. Tregenna-Piggott, H. Weihe, J. Bendix, A.-L. Barra, H.-U. Güdel, Inorg. Chem. 38 (1999) 5928.
[18] P.L.W. Tregenna-Piggott, H. Weihe, A.-L. Barra, Inorg. Chem. 42 (2003) 8504.
[19] W.H. Press, B.P. Flannery, A.A. Teukolsky, W.T. Vetterling, Numerical Recipes in Pascal, Cambridge University Press, Cambridge, 1989, p. 572.
[20] J. Krzystek, S.A. Zvyagin, A. Ozarowski, S. Trofimenko, J. Telser, J. Magn. Reson. 178 (2006) 174.
[21] G. Kozlov, A. Volkov, in: G. Grüner (Ed.), Topics in Applied Physics: Millimeter and Submillimeter Wave Spectroscopy of Solids, Springer, Berlin, 1998, p. 51.
[22] G.M. Zverev, A.M. Prokhorov, Sov. Phys. JETP 11 (1960) 330.
[23] S. Foner, W. Low, Phys. Rev. 120 (1960) 1585.
[24] M. Sauzade, J. Pontnau, P. Lesas, D. Silhouette, Phys. Lett. 19 (1966) 617.
[25] R.R. Joyce, P.L. Richards, Phys. Rev. 179 (1969) 375.

[26] P.L.W. Tregenna-Piggott, S.P. Best, H.-U. Güdel, H. Weihe, C.C. Wilson, J. Solid State Chem. 145 (1999) 460.
[27] P.L.W. Tregenna-Piggott, D. Spichiger, G. Carver, B. Frey, R. Meier, H. Weihe, J.A. Cowan, G.J. McIntyre, G. Zahn, A.-L. Barra, Inorg. Chem. 43 (2004) 8049.
[28] P.L.W. Tregenna-Piggott, G. Carver, Inorg. Chem. 43 (2004) 8061.
[29] S. Dolder, D. Spichiger, P.L.W. Tregenna-Piggott, Inorg. Chem. 42 (2003) 1343.
[30] J. Krzystek, A.T. Fiedler, J.J. Sokol, A. Ozarowski, S.A. Zvyagin, T.C. Brunold, J.R. Long, L.-C. Brunel, J. Telser, Inorg. Chem. 43 (2004) 5645.
[31] N. Laurance, J. Lambe, Phys. Rev. 132 (1963) 1029.
[32] C.J.H. Jacobsen, E. Pedersen, J. Villadsen, H. Weihe, Inorg. Chem. 32 (1993) 1216.
[33] J. Krzystek, J. Telser, unpublished observations.
[34] R.M. Macfarlane, J. Chem. Phys. 42 (1964) 442.
[35] G. Elbers, S. Remme, G. Lehmann, Inorg. Chem. 25 (1986) 896.
[36] E. Pedersen, H. Toftlund, Inorg. Chem. 13 (1974) 1603.
[37] G.S. Shakurov, V.F. Tarasov, Appl. Magn. Reson. 21 (2001) 597.
[38] K. Ono, S. Koide, H. Sekiyama, H. Abe, Phys. Rev. 96 (1954) 38.
[39] K. Ono, J. Phys. Soc. Jpn. 12 (1957) 1231.
[40] J. Telser, L.A. Pardi, J. Krzystek, L.-C. Brunel, Inorg. Chem. 37 (1998) 5769.
[41] J. Telser, L.A. Pardi, J. Krzystek, L.-C. Brunel, Inorg. Chem. 39 (2000) 1834.
[42] V.F. Tarasov, G.S. Shakurov, B.Z. Malkin, V.A. Ulanov, in: C.Z. Rudowicz (Ed.), Modern applications of EPR/ESR, Springer, Singapore, 1998.
[43] M.M. Zaripov, V.F. Tarasov, V.A. Ulanov, G.S. Shakurov, Phys. Solid State 44 (2002) 2050.
[44] M.M. Zaripov, V.F. Tarasov, V.A. Ulanov, G.S. Shakurov, M.L. Popov, Phys. Solid State 37 (1995) 437.
[45] D.P. Goldberg, J. Telser, J. Krzystek, A.G. Montalban, L.-C. Brunel, A.G.M. Barrett, B.M. Hoffman, J. Am. Chem. Soc. 119 (1997) 8722.
[46] J. Krzystek, J. Telser, L.A. Pardi, D.P. Goldberg, B.M. Hoffman, L.-C. Brunel, Inorg. Chem. 38 (1999) 6121.
[47] J. Krzystek, L.A. Pardi, L.-C. Brunel, D.P. Goldberg, B.M. Hoffman, S. Licoccia, J. Telser, Spectrochim. Acta A 58 (2002) 1113.
[48] J. Krzystek, J. Telser, J. Magn. Reson. 162 (2003) 454.
[49] J. Bendix, H.B. Gray, G. Golubkhov, Z. Gross, Chem. Commun. (2000) 1957.
[50] J. Krzystek, J. Telser, B.M. Hoffman, L.-C. Brunel, S. Licoccia, J. Am. Chem. Soc. 123 (2001) 7890.
[51] D.E. Lansky, B. Mandimutsira, B. Ramdhanie, M. Clausen, J. Penner-Hahn, S.A. Zvyagin, J. Telser, J. Krzystek, R. Zhang, Z. Ou, K.M. Kadish, L. Zhakarov, A.L. Rheingold, D.P. Goldberg, Inorg. Chem. 44 (2005) 4485.
[52] J.D. Harvey, C.J. Ziegler, J. Telser, A. Ozarowski, J. Krzystek, Inorg. Chem. 44 (2005) 4451.
[53] H.J. Gerritsen, E.S. Sabisky, Phys. Rev. 132 (1963) 1507.
[54] A.-L. Barra, D. Gatteschi, R. Sessoli, G.L. Abbati, A. Cornia, A.C. Fabretti, M.G. Uytterhoeven, Angew. Chem. Int. Ed. 36 (1997) 2329.
[55] J. Krzystek, G. Yeagle, J.-H. Park, M.W. Meisel, R.D. Britt, L.-C. Brunel, J. Telser, Inorg. Chem. 42 (2003) 4610.
[56] G. Aromí, J. Telser, A. Ozarowski, L.-C. Brunel, J. Krzystek, Inorg. Chem. 44 (2005) 187.
[57] A.K. Gregson, D.M. Doddrell, P.C. Healy, Inorg. Chem. 17 (1978) 1216.
[58] I. Krivokapič, C. Noble, S. Klitgaard, P.L.W. Tregenna-Piggott, H. Weihe, A.-L. Barra, Angew. Chem. Int. Ed. 44 (2005) 3613.
[59] J. Krzystek, J. Telser, M.J. Knapp, D.N. Hendrickson, G. Aromí, G. Christou, A. Angerhofer, L.-C. Brunel, Appl. Magn. Reson. 23 (2001) 571.
[60] S. Kimura, T. Otani, Y. Narumi, K. Kindo, M. Nakano, G. Matsubayashi, J. Magn. Magn. Mater. 272–276 (2004) 1102.
[61] J. Limburg, J.S. Vrettos, R.H. Crabtree, G.W. Brudvig, J.C. de Paula, A. Hassan, A.-L. Barra, C. Duboc-Toia, M.-N. Collomb, Inorg. Chem. 40 (2001) 1698.
[62] C. Mantel, A.K. Hassan, J. Pécaut, A. Deronzier, M.-N. Collomb, C. Duboc-Toia, J. Am. Chem. Soc. 125 (2003) 12337.
[63] S. Mossin, H. Weihe, A.-L. Barra, J. Am. Chem. Soc. 124 (2002) 8764.
[64] S. Mossin, M. Stefan, P. ter Heerdt, A. Bouwen, E. Goovaerts, H. Weihe, Appl. Magn. Reson. 21 (2001) 587.
[65] J.C. Hempel, J. Chem. Phys. 64 (1976) 4307.
[66] J.C. Hempel, R.A. Palmer, M.C.-L. Yang, J. Chem. Phys. 64 (1976) 4314.
[67] W.B. Lynch, R.S. Boorse, J.H. Freed, J. Am. Chem. Soc. 115 (1993) 10909.
[68] R.M. Wood, D.M. Stucker, L.M. Jones, W.B. Lynch, S.K. Misra, J.H. Freed, Inorg. Chem. 38 (1999) 5384.
[69] S.K. Misra, S.I. Andronenko, K.A. Earle, J.H. Freed, Appl. Magn. Reson. 21 (2001) 549.
[70] S.K. Misra, S.I. Andronenko, G. Rinaldi, P. Chand, K.A. Earle, J.H. Freed, J. Magn. Reson. 160 (2003) 131.
[71] S.K. Misra, S.I. Andronenko, P. Chand, K.A. Earle, S.V. Paschenko, J.H. Freed, J. Magn. Reson. 174 (2005) 265.
[72] H. Hori, M. Ikeda-Saito, G.H. Reed, T. Yonetani, J. Magn. Reson. 58 (1984) 177.
[73] C. Mantel, C. Baffert, I. Romero, A. Deronzier, J. Pécaut, M.-N. Collomb, C. Duboc, Inorg. Chem. 43 (2004) 6455.
[74] B.J. Gaffney, C. Su, E.H. Oliw, Appl. Magn. Reson. 21 (2001) 411.
[75] S. Un, P. Dorlet, G. Voyard, L.C. Tabares, N. Cortez, J. Am. Chem. Soc. 123 (2001) 10123.
[76] S. Un, L.C. Tabares, N. Cortez, B.Y. Hiraoka, F. Yamakura, J. Am. Chem. Soc. 126 (2004) 2720.
[77] L.C. Tabares, N. Cortez, I. Agalidis, S. Un, J. Am. Chem. Soc. 127 (2005) 6039.
[78] J.R. Pilbrow, Transition Ion Electron Paramagnetic Resonance, Clarendon Press, Oxford, 1990.
[79] B.D. Abraham, M. Sono, O. Boutaud, A. Shriner, J.H. Dawson, A.R. Brash, B.J. Gaffney, Biochemistry 40 (2001) 2251.
[80] P.J.M. van Kan, E. van der Horst, E.J. Reijerse, P.J.M. van Bentum, W.R. Hagen, J. Chem. Soc. Faraday Trans. 94 (1998) 2975.
[81] K.K. Andersson, P.P. Schmidt, B. Katterle, K.R. Strand, A.E. Palmer, S.-K. Lee, E.I. Solomon, A. Gräslund, A.-L. Barra, J. Biol. Inorg. Chem. 8 (2003) 235.
[82] For actual spectra, see J. Krzystek, L.C. Brunel, J.M. Nocek, J. Telser, B.M. Hoffman, 2002 NHMFL Annual Research Review, p. 74, available on-line from: http://www.magnet.fsu.edu/publications/2002annualreview.
[83] A. Sienkiewicz, J. Krzystek, B. Vileno, G. Chatain, A.J. Kosar, D.S. Bohle, L. Forro, J. Am. Chem. Soc. 128 (2006) 4534.
[84] S. Pagola, P.W. Stephens, D.S. Bohle, A.D. Kosar, S.K. Madsen, Nature 404 (2000) 307.
[85] P.L. Richards, W.S. Caughey, H. Eberspaecher, G. Feher, M. Malley, J. Chem. Phys. 47 (1967) 1187.
[86] G.C. Brackett, P.L. Richards, W.S. Caughey, J. Chem. Phys. 54 (1971) 4383.
[87] R. Aasa, J. Chem. Phys. 52 (1970) 3919.
[88] J.P. Renault, C. Verchere-Beaur, I. Morgenstern-Badarau, F. Yamakura, M. Gerloch, Inorg. Chem. 39 (2000) 2666.
[89] H. Meštric, R.-A. Eichel, K.-P. Dinse, A. Ozarowski, J. van Tol, L.-C. Brunel, J. Appl. Phys. 96 (2004) 7440.
[90] F. Di Benedetto, G. Andreozzi, G. Baldi, A. Barzanti, G.P. Bernardini, V. Faso, L.A. Pardi, M. Romanelli, J. Eur. Ceramic Soc., doi:10.1016/j.jeurceramsoc.2005.04.007.
[91] A.M. Ferretti, A.-L. Barra, L. Forni, C. Oliva, A. Schweiger, A. Ponti, J. Phys. Chem. B 108 (2004) 1999.
[92] A. Priem, P.J.M. van Bentum, W.R. Hagen, E.J. Reijerse, Appl. Magn. Reson. 21 (2001) 535.
[93] J. Telser, J. van Slageren, S. Vongtragool, M. Dressel, W.M. Reiff, S.A. Zvyagin, A. Ozarowski, J. Krzystek, Magn. Reson. Chem. 43 (2005) S130.
[94] A. Ozarowski, S.A. Zvyagin, W.M. Reiff, J. Telser, L.-C. Brunel, J. Krzystek, J. Am. Chem. Soc. 126 (2004) 6574.

[95] P.M. Champion, A.J. Sievers, J. Chem. Phys. 66 (1977) 1819.
[96] M.J. Knapp, J. Krzystek, L.-C. Brunel, D.N. Hendrickson, Inorg. Chem. 39 (2000) 281.
[97] E. Münck, K.K. Surerus, M.P. Hendrich, Methods Enzymol., Part D 227 (1993) 463.
[98] K. Ray, A. Begum, T. Weyhermuller, S. Piligkos, J. van Slageren, F. Neese, K. Wieghardt, J. Am. Chem. Soc. 127 (2005) 4403.
[99] L.J. Guggenberger, C.T. Prewitt, P. Meakin, S. Trofimenko, J.P. Jesson, Inorg. Chem. 12 (1973) 508.
[100] A. Bencini, D. Gatteschi, Inorg. Chem. 16 (1977) 2141.
[101] R.P. van Stapele, H.G. Beljers, P.F. Bongers, H. Zijlstra, J. Chem. Phys. 44 (1966) 3719.
[102] J. Krzystek, S.A. Zvyagin, A. Ozarowski, A.T. Fiedler, T.C. Brunold, J. Telser, J. Am. Chem. Soc. 126 (2004) 2148.
[103] J. Krzystek, L.-C. Brunel, J. Telser, 2001 NHMFL Annual Research Review, p. 54, available on-line from: http://www.magnet.fsu.edu/publications/2001annualreview.
[104] J. Krzystek, J.-H. Park, M.W. Meisel, M.A. Hitchman, H. Stratemeier, L.-C. Brunel, J. Telser, Inorg. Chem. 41 (2002) 4478.
[105] J. Telser, J. Krzystek, S.A. Zvyagin, A. Ozarowski, R. Wagner, K.O. Christe, J.R. Boatz, 2004 NHMFL Annual Research Report #27, available on-line from: http://www.magnet.fsu.edu/publications/2004annualreport.
[106] K. Ono, J. Phys. Soc. Jpn. 8 (1953) 802.
[107] D. Collison, M. Helliwell, V.M. Jones, F.E. Mabbs, A.J.L. McInnes, P.C. Riedi, G.M. Smith, R.G. Pritchard, W.I. Cross, J. Chem. Soc., Faraday Trans. 94 (1998) 3019.
[108] P.J. van Dam, A.A.K. Klaassen, E.J. Reijerse, W.R. Hagen, J. Magn. Reson. 130 (1998) 140.
[109] J. Mrozinski, A. Skorupa, A. Pochaba, Y. Dromzee, M. Verdaguer, E. Goovaerts, H. Varcammen, B. Korybut-Daszkiewicz, J. Mol. Struct. 559 (2001) 107.
[110] L.A. Pardi, A.K. Hassan, F.B. Hulsbergen, J. Reedijk, A.L. Spek, L.-C. Brunel, Inorg. Chem. 39 (2000) 159.
[111] E.-C. Yang, C. Kirman, J. Lawrence, L.N. Zakharov, A.L. Rheingold, S. Hill, D.N. Hendrickson, Inorg. Chem. 44 (2005) 3827.
[112] E. Wasserman, L.C. Snyder, W.A. Yager, J. Chem. Phys. 41 (1964) 1763.
[113] P. Kottis, R. Lefebvre, J. Chem. Phys. 41 (1964) 379.
[114] G. Rogez, J.-N. Rebilly, A.-L. Barra, L. Sorace, G. Blondin, N. Kirchner, M. Duran, J. van Slageren, S. Parsons, L. Ricard, A. Marvilliers, T. Mallah, Angew. Chem. Int. Ed. 44 (2005) 1876.
[115] S. Vongtragool, B. Gorshunov, M. Dressel, J. Krzystek, D.M. Eichhorn, J. Telser, Inorg. Chem. 42 (2003) 1788.
[116] R. Miyamoto, S. Sudoh, in: C.Z. Rudowicz (Ed.), Modern Applications of EPR/ESR, Springer, Singapore, 1998.
[117] R.B. Clarkson, A.I. Smirnov, T.I. Smirnova, H. Kang, R.L. Belford, K. Earle, J.H. Freed, Mol. Phys. 95 (1998) 1325.
[118] R. Basler, P.L.W. Tregenna-Piggott, H. Andres, C. Dobe, H.-U. Güdel, S. Janssen, G.J. McIntyre, J. Am. Chem. Soc. 123 (2001) 3377.
[119] M.M. Zaripov, V.F. Tarasov, V.A. Ulanov, G.S. Shakurov, M.L. Popov, Phys. Solid State 38 (1996) 249.